The impact of distinct cholinergic neuronal populations on amygdala circuits and learning related behavior

Teemu Aitta-Aho, Y. Audrey Hay, Benjamin Phillips, Lisa Saksida, Tim Bussey, Ole Paulsen, John Apergis-Schoute

Article

The impact of distinct cholinergic neuronal populations on amygdala circuits and learning-related behavior

Teemu Aitta-aho[1,2,8], Y Audrey Hay[3,8], Benjamin U. Phillips[4], Lisa M. Saksida[4,5,6], Tim J. Bussey[4,5,6], Ole Paulsen[3] and John Apergis-Schoute*[1,7]

[1] Department of Pharmacology, University of Cambridge, Cambridge, CB2 1PD, UK.
[2] Department of Pharmacology, Faculty of Medicine, University of Helsinki, 00014 Helsinki, Finland
[3] Department of Physiology, Development, and Neuroscience, University of Cambridge, Cambridge,CB2 3DY, UK.
[4] Department of Psychology, University of Cambridge, Cambridge, CB2 3RQ, UK.
[5] Robarts Research Institute, Schulich School of Medicine and Dentistry, Western University, London, ON, Canada
[6] Canada Brain and Mind Institute, Western University, London, ON, Canada
[7] Department of Neuroscience, Psychology and Behaviour, University of Leicester, Leicester LE1 7RH, UK
[8] Contributed equally to the work

Running Title: Cholinergic control of amygdala function

*Corresponding and Lead Author:
Dr. John Apergis-Schoute
Email: iea6@le.ac.uk

Neuroscience, Psychology and Behaviour
University of Leicester
University Road
Leicester LE1 7RH

Number of pages:		43
Number of illustrations and tables:	- Figures	6
	-Supplementary Figures	8
	- Tables	0
	- Multimedia	0
	- 3D models	0

.

Summary:

The central cholinergic system and the amygdala are well-known to be important for motivation and mnemonic processes. Different cholinergic populations innervate the amygdala but it is unclear how these projections impact amygdala activity and behavior. Using optogenetic circuit-mapping strategies in ChAT-cre mice we demonstrate that amygdala-projecting basal forebrain and brainstem ChAT-containing neurons can differentially affect amygdala circuits and behavior. Photoactivating ChAT terminals *in vitro* revealed the underlying synaptic impact of brainstem inputs to the central lateral division to be excitatory, mediated via the synergistic glutamatergic activation of AMPA and NMDA receptors. In contrast, stimulating NBm-ChAT inputs to the basal nucleus resulted in endogenous ACh release resulting in muscarinic receptor dependent biphasic inhibition-excitation responses onto principal neurons. Such a biphasic inhibitory-excitatory response profile is a physiological hallmark of neural oscillations and could thus form the basis of acetylcholine-mediated rhythmicity in amygdala networks. Consistent with this, *in vivo* NBm activation strengthened amygdala basal nucleus theta and gamma frequency rhythmicity, both of which continued for seconds after stimulation. Stimulation-evoked and ongoing increases in gamma and theta power were dependent on local nicotinic or muscarinic receptor activation, respectively. Activation of brainstem ChAT-containing neurons however resulted in a transient increase in central lateral amygdala network synchrony that was independent of cholinergic receptors. In addition, driving these respective inputs in behaving animals induced opposing appetitive and defensive learning-related behavioral changes. Since learning and memory is supported by both cellular and network-level processes in central cholinergic and amygdala networks, these results provide a route by which distinct cholinergic inputs can convey salient information to the amygdala and promote associative biophysical changes that underlie amygdala-dependent memories.

Introduction:

Effective learning requires attending selectively to information while ignoring distractions [1]. The capacity of a stimulus to capture attention can be attributed to the stimulus' saliency or features that make it stand out among other stimuli [2]. Both central cholinergic systems [4,5] and the amygdala [5,6] are important for saliency detection and attention - two processes that are critical for effective learning and memory [7-9]. Disruptions in these functions are common in diseases that severely affect memory, as is the case in Alzheimer's disease [10]. In addition to declarative memory deficits, Alzheimer's disease patients show severe impairments in emotional memory [11,12] - a phenotype that may be due to a significant neuronal loss in amygdala and central cholinergic cell populations [11,13,14]. Such relations between circuit-level degeneration and disturbances in cognition underscore the clinical significance of interactions between acetylcholine (ACh) and amygdala networks.

Mechanistically, central ACh can strengthen attention by enhancing the gain of sensory signaling resulting in an increase in neuronal responding to salient stimuli [15-18]. Moreover, by synchronizing activity within and between neural networks [19-21], ACh can support attentional [22,23] and mnemonic [7] processes and, on the cellular level, promote synaptic plasticity [24,25]. Distinct central cholinergic populations residing in the basal forebrain (NBm) and the pedunculopontine tegmental nucleus (PPT) of the brainstem show overlapping functions as both contribute to attention and motivation [26,27]. Moreover, individual NBm neurons have been shown to respond to natural and learned emotionally-salient stimuli [28-30] and can do so on the order of tens of milliseconds [31]. These results suggest that, in addition to responding to salient simuli, NBm neurons are positioned to quickly communicate information regarding the incentive value of stimuli to target regions. Brainstem neurons similarly encode for stimuli with motivational significance since a subpopulation of PPT neurons respond to salient cues while other PPT neurons transiently discharge in response to reward delivery [32].

Both cholinergic NBm [33] and PPT populations [34,35] innervate the amygdala, a collection of limbic nuclei that act cooperatively to establish associative links between neutral environmental stimuli and ones with intrinsic positive or negative valence [36]. Neurons in the basolateral nucleus of the amygdala (BL) encode for rewarding and aversive stimuli [37,38] and have been shown to update their activity when stimulus valence is modified [38,39]. Similar to the amygdala, PPT neurons respond to salient stimuli [32] and intact PPT functioning has been linked to associative learning [40]. Despite these anatomical and functional relationships, the impact of distinct cholinergic populations on amygdala processes has not been thoroughly compared and contrasted. Moreover, it is unclear whether the synaptic organization of ACh inputs to the amygdala can support rhythmic neural activity

as they do in other memory-related brain regions. Increased synchrony in amygdala circuits has been linked to innate [41,42] and learned emotional responses [43,44] but the neural mechanisms mediating this network-level rhythmicity are currently unresolved.

To shed light on the cholinergic influences on amygdala activity and function this study has implemented optogenetic circuit mapping methods in transgenic ChAT-cre mice to determine the anatomical, synaptic, network-level, and behavioral impact of basal forebrain and brainstem cholinergic cell populations on identified amygdala circuits. We show that distinct cholinergic NBm and brainstem ACh populations send axons to the basal (BL) and central lateral (CeL) amygdala nuclei, respectively, functionally impacting BL and CeL circuits. NBm-ChAT activation can synchronize ongoing BL activity through cholinergic transmission while PPT-ChAT activation can transiently drive amygdala activity via glutamatergic neurotransmission. Behaviorally, photo-activating BL- and CeL-projecting ChAT pathways were seen to drive appetitive and defensive responses. Collectively, these results highlight the unique role of distinct central cholinergic systems on amygdala circuits and function.

Results:

Non-overlapping innervation of amygdala nuclei by distinct cholinergic cell populations

Cholinergic fibers emanating from the NBm [33], the rodent homologue of Meynert's basal nucleus of primates, and PPT [34,35], are known to project to the amygdala but the topographical organization of ACh-amygdala projections has not been thoroughly delineated. To investigate the functional connectivity of cholinergic inputs to the amygdala we used a cre-recombinase approach in transgenic ChAT-cre mice to express channelrhodopsin (ChR2) linked to GFP proteins in NBm and PPT cholinergic populations and their axonal processes (Fig 1). Immunohistological analysis of cre-dependent expression of GFP revealed that labeled NBm and PPT neurons were also immuno-positive for the ACh enzyme ChAT (GFP labeled neurons co-expressing ChAT, NBm: n = 3 mice, 96.4 ± 1.3%, 172 cells; PPT: n = 4 mice, 89.2 ± 4.9% 117 cells). (Fig S1). Axons from NBm-ChAT neurons densely innervated the BL and central medial (CeM) divisions of the amygdala leaving the LA and CeL nuclei remarkably devoid of NBm-ACh inputs (Fig 1B,C). In contrast, PPT-ChAT neurons almost exclusively innervated the CeL nucleus (Fig 1E,F). Taken together, these anatomical results reveal a striking non-overlapping and complementary innervation of different amygdala nuclei by distinct ACh populations.

***In vivo* photo-activation of NBm-ChAT neurons synchronizes BL activity for seconds after stimulation while PPT-ChAT neurons transiently activate CeL networks**

We next went on to characterize how stimulating NBm and PPT cholinergic neurons impacts network activity in the BL and CeL, respectively. We simultaneously recorded NBm and BL or PPT and CeL local field potential (LFP) and multi-unit (MUA) activity in anesthetized ChAT-cre mice either injected with an adeno-associated virus containing the ChR2 sequence or crossed with Ai32 reporter line. Under urethane anesthesia, LFP activity in the NBm and BL exhibited slow oscillations (<1Hz) (Fig 2A) characteristic of slow-wave sleep and episodes of desynchronized activity. We measured the response to photo-activation (5-7 pulses at 20Hz repeated every 40 seconds) of NBm-ChAT or PPT-ChAT circuits, respectively. As expected, light bursts in NBm-ChAT circuits increased the power intensity of the LFP most profoundly in the slow gamma range (20-30 Hz), corresponding to the photo-stimulation frequency (Fig 2A; 2B, blue trace). This oscillatory activity continued in the absence of photo-stimulation resulting in a broad increase of NBm power intensity in theta (4-16Hz) and gamma (20-60Hz) that decayed following stimulation (Fig 2A; 2B, red trace). Simultaneous LFP recordings made from the BL showed a similar marked increase of theta and slow gamma during NBm-ChAT stimulation (Fig 2C; 2D, blue trace) that remarkably persisted and increased in power after stimulation had ended (Fig 2C, 2D, red trace). Similar BL responses evoked by NBm-ChAT stimulation were recorded in awake mice (n = 4) albeit of a smaller magnitude (Fig S4).

In response to stimulation of PPT ChAT-containing neurons, PPT (Fig 2F) and CeL (Fig 2H) circuits showed time-locked responses to the photo-activation frequency (20 Hz). In contrast to the NBm to BL pathway, PPT-induced CeL activity was greater during the stimulation than after (Fig 2D, 2I) revealing, in comparison to NBm-ChAT projections to the BL, a more temporally restricted influence on CeL networks. The recorded LFPs were likely due to local changes in amygdala activity as NBm- and PPT-ChAT neuronal activation led to an increase in BL (Fig 2E) and CeL (Fig 2J) MUA, respectively. Taken together, these *in vivo* results indicate that 20 Hz activation of NBm-ACh circuits can effectively synchronize BL networks, persisting for seconds in the absence of stimulation, while PPT activation mostly influences CeL neurons during PPT-ChAT activation. Collectively, by assessing the functional connectivity between cholinergic nuclei and amygdala targets these results demonstrate that two separate ACh pathways are positioned to distinctly influence amygdala network activity.

XX

NBm-ChAT neurons trigger a M1-mediated biphasic activation of BL network while PPT-ChAT neurons influence CeL dynamics through AMPAR and NMDAR activation

We next investigate the cellular mechanisms underlying these unique responses by recording in acute slices the responses of BL and CeL neurons to photo-stimulation of NBm- (Fig 3A-H) and PPT-ChAT (Fig 3I-N) populations, respectively. Current-clamp recordings of BL principal cells show that photo-stimulating NBm-ChAT inputs to the BL effectively suppressed amygdala activity (n=29 out 41 cells, Fig 3D), as reported previously [45,46]. This response persisted in the presence of glutamate (AMPA

(CNQX, 20 ⌈M), NMDA (AP-5, 100 ⌈M)) and $GABA_{A,B}$ (gabazine 10 ⌈M; CGP-52432 10 ⌈M) receptor blockers (Fig S3A) and occurred with a similar latency in baseline and network antagonist blockers (n=11 cells, 43.3 ± 2.5 ms and 40.7 ± 3.1 ms after stimulation, Wilcoxon Signed Rank Test, p = 0.65). Furthermore, the inhibitory response reversed at -90 mV (n=6) (Fig S2A, was insensitive to the SK channel blocker apamin (% of baseline, 96.1 ± 3.2%; n = 5; Wilcoxon Signed Rank Test, p = 0.38; Fig. S2B) but was abolished by application of the muscarinic M1 receptor (M1R)-antagonist pirenzepine (PRZ) (n = 8 cells: 1 ⌈M; Amplitude: ctl, 9.4 ± 1.6 pA; PRZ, 1.4 ± 0.3 pA; Wilcoxon Signed Rank Test; p = 0.001; Fig 3E; S3C). These results indicate that photo-activation of NBM-ChAT inputs trigger a K^+-mediated inhibitory conductance via the activation of M1Rs. Moreover, with only glutamate and $GABA_A$ receptor antagonists present, application of baclofen (BFN), a $GABA_B$ antagonist known to activate GIRK channels, prevented the inhibitory response to photo-stimulation to occur (2.1 ± 4.0% of control response, n=6 cells, Wilcoxon Signed Rank Test, p = 0.04; Fig 3G), indicating that the M1R-dependent inhibition is mediated through activation of GIRK channels - a result consistent with the findings of Unal et al. (2015).

The BL contains a relatively high degree of acetylcholinesterase (AChE), the enzyme that catalyzes the breakdown of endogenous ACh, suggesting that BL cholinergic transmission is spatially and temporally under tight regulatory control. It is thus conceivable that the NBm-ChAT mediated inhibition of BL principal neurons may in fact be due to the fast and reliable release of ACh. To test this hypothesis we evoked inhibitory responses with minimal light stimulation (0.5 ms) in the presence of synaptic antagonists while bath-applying the AChE inhibitor physostigmine (Phys) (Fig S3C). Blocking ACh breakdown with 10 μM phys led to an increase in the amplitude and duration of NBm-ACh-evoked inhibition (n = 6 cells: Amplitude: ctl, 9.6 ± 1.6 pA; physo, 25.9 ± 6.1 pA. Duration: ctl, 0.08 ± 0.02 s; physo, 1.23 ± 0.34 s) (Fig 3B3,4). The inhibitory responses were completely blocked by the M1R antagonist PRZ (1 μM) (Fig 3B3,4) (Amplitude: ctl, 9.6 ± 1.6 pA; PRZ, 1.9 ± 0.5 pA; washout, 6.2 ± 1.2 pA. Duration: ctl, 0.08 ± 0.02 s; PRZ, 0.03 ± 0.01 s s; washout 0.07 ± 0.03) (Amplitude: One-way ANOVA; F(3,18) = 9.4 p = 0.0005, Bonferroni post-hoc test, Control vs. physo p = 0.0008, Control vs. PRZ p = 0.01, physo vs. PRZ/washout p = 0.004 PRZ vs. washout p = 0.01. Decay Time: One-way ANOVA; F(3,18) = 2.28 p = 0.0001, Bonferroni post-hoc test, Control vs. physo p = 0.0006, Control vs. PRZ p = 0.01, physo vs. PRZ/washout p = 0.0002 PRZ vs. washout p = 0.01). These results are consistent with previous studies demonstrating an increase in M1-dependent K^+-conductance in BL principal neurons to pressure injections of ACh [47,48].

In addition to the inhibitory responses triggered by a single pulse of light, current-clamp recordings showed that during a train of stimulation (20 Hz) a biphasic response developed with the initial inhibitory response being followed by an excitatory component (Fig S2D, 3F – black trace). This

excitatory component was also abolished by the M1R antagonist PRZ (7.3 ± 1.4% of control current, n = 8 cells, Wilcoxon Signed Rank Test, p = 0.008; Fig 3F – red trace), indicating that both currents were elicited by M1R activation. To test whether this M1R-mediated depolarization was independent of the preceding inhibition we used an occlusion strategy, which consists of maximally activating the K^+ channels mediating the M1R inhibitory response. Photo-stimulation while blocking $GABA_B$ receptor linked GIRK channels resulted in a purely delayed excitatory response (Fig 3H), confirming that GIRK channels mediate the inhibitory response while demonstrating an independent NBm-ChAT mediated excitation of BL principal neurons.

In contrast to NBm-BL pathways, stimulation of the PPT-ChAT (Fig 3I) fibers elicited short latency inward currents in CeL neurons recorded in voltage-clamp mode (n = 19 cells: Amplitude: 24.3 ± 4.5 pA, Latency: 4.2 ± 0.2 ms). Photo-induced currents were completely abolished by bath-application of the AMPA receptor antagonist CNQX (Fig 3K), suggesting for a PPT glutamatergic influence onto postsynaptic CeL targets. Such a mechanism is not extraordinary since PPT [49] and other cholinergic populations have been shown to use glutamate as a neurotransmitter [50]. Approximately 70% of PPT-ChAT connected CeL neurons showed signature late-spiking properties. We then investigated the respective roles of AMPAR and NMDAR activation during a train of stimulus (20 Hz during 20 sec). Photo-stimulation led to a significant increase in CeL neuronal firing that outlasted the stimulation duration (Fig 3L-left). While the initial depolarization was dependent of AMPA receptor activation (Fig 3L-middle), the long-lasting increase in excitability was sensitive to the NMDA antagonist AP-V (100 ⌈M) (Fig 3L-right) (n = 7 cells: ctl, 7.4 ± 0.5 mV; CNQX, 3.9 ± 0.3 mV; AP-V, 0.5 ± 0.2 mV; One-way ANOVA F(1.57, 9.43) = 128.9, p = 0.0001; Bonferroni post-hoc test, Control vs. cnqx p = 0.0009, Control vs. AP-V p = 0.0001, CNQX vs. AP-V p = 0.0007). The NMDA response was mostly absent at more negative membrane potentials (Fig 3M), suggesting for cooperative interactions between AMPA and NMDA receptors at depolarized membrane potentials. Because PPT neurons are active in a range of frequencies [51], we next tested the influence of frequency stimulation on CeL neurons (Fig 3N). Activation of PPT-ChAT terminals could equally excite CeL neurons with 10 and 20 Hz stimulation while 5 Hz stimulation activated CeL neurons to a lesser extent (n = 8 cells: 20 Hz, 5.7 ± 0.7 mV, n = 8; 10 Hz, 5.3 ± 0.4 mV, n = 8; 5 Hz, 2.9 ± 0.7 mV, n = 5; Two-way ANOVA F(2, 19) = 6.93, p = 0.005; Bonferroni post-hoc test, 20Hz vs. 10Hz p = 0.82, 20Hz vs. 5Hz p = 0.01, 10Hz vs. 5Hz p = 0.02). These responses were insensitive to either muscarinic (atropine (ATR), 2 ⌈M, 98.1 ± 6.34% of control response, n = 5 cells; Wilcoxon Signed Rank Test, p = 0.57) or nicotinic (mecamylamine (MEC), 10 ⌈M, 104.3 ± 3.71% of control response, n = 8 cells; Wilcoxon Signed Rank Test, p = 0.36) receptor antagonists (Fig S4A-C) and bath application of ACh (100⌈M) did not affect CeL neurons membrane potential in current-clamp mode (baseline, -75.1 ± 2.4 mV; ACh, -73.6 ± 2.5, n = 8 cells, Wilcoxon Signed Rank Test, p = 0.11) (Fig S4D,E). These findings

provide evidence that PPT ChAT-containing neurons are capable of exciting CeL neurons through glutamate release that is independent of ACh transmission *in vitro*.

NBm-ChAT mediated increases in BL network rhythmicity requires acetylcholine receptor activation while PPT-ChAT evoked CeL activity is independent of cholinergic transmission

The above results demonstrate that NBm- and PPT-ChAT have a strikingly different mechanism of action on BL and CeL networks, respectively. It remains unclear however whether direct activation of muscarinic receptor is the main mode of activation of BL network *in vivo*, and whether there is a cholinergic component of PPT-mediated activation of CeL circuits *in vivo* that was not be detectable in slice. We next tested the effects of i.p. injections of ACh antagonists on NBm-ChAT photo-activation on BL activity *in vivo* (Fig S5). As shown earlier, photo-stimulating NBm-ChAT neurons at 20 Hz led to increase in the magnitude of BL oscillations in the theta (n = 6 mice: 5-15 Hz, 1.29 ± 0.03 of baseline), low (15-50 Hz, 1.74 ± 0.04 of baseline) and high (50-100 Hz, 1.51 ± 0.04 of baseline) gamma frequencies (Fig S5D, open circles). Following a drug-free baseline recording, mice were injected i.p. with 4 mg/kg Scopolamine (SCP) and 2 mg/kg MEC and the stimulation/recording was repeated. MEC + SCP i.p. injections did not significantly affect local NBm 20 Hz activity (n = 6 mice: Ctl, 736 ± 16 μV^2/Hz; MEC + SCP, 783 ± 18 μV^2/Hz; Wilcoxon signed-rank test, p = 0.22) (Fig S5B). In contrast, ACh receptor antagonists (MEC + SCP) significantly reduced NBm-ChAT evoked theta (n = 6 mice: Ctl, 1.29 ± 0.03; MEC+SCP, 1.03 ± 0.01 of baseline; Wilcoxon signed-rank test, p = 0.03), low (Ctl, 1.74 ± 0.04; MEC+SCP, 1.12 ± 0.02 of baseline; Wilcoxon signed-rank test, p = 0.03) and high gamma power (Ctl, 1.51 ± 0.04; MEC+SCP, 1.09 ± 0.02 of baseline; Wilcoxon signed-rank test, p = 0.03) in the BL (Fig S5D).

Following from our *in vitro* data showing that NBm-ChAT modulation of BL neuron activity is via M1Rs, we next repeated NBm and BL recordings but with local BL infusions (0.7 μL) of the muscarinic receptor antagonist ATR (Fig 4). Our analysis revealed that local BL infusions of ATR disrupted NBm-ChAT induced BL theta specifically following the stimulation (n = 6 mice: Ctl, 1.46 ± 0.10; ATR, 1.12 ± 0.03; Wilcoxon signed-rank test, p = 0.03) (Fig 4E,F) while having no effect on the 20 Hz responses in the NBm (n = 5 mice; Ctl, 715.6 ± 236.6 μV^2/Hz; ATR, 737.6 ± 270.6 μV^2/Hz); Wilcoxon signed-rank test, p = 0.76) (Fig 4B), suggesting for a selective muscarinic role in BL theta activity that outlasts NBm-ChAT stimulation. In contrast, local BL infusions of MEC (0.02 ng) had no effect on theta (n = 6 mice: stim; Ctl, 1.45 ± 0.10, MEC, 1.28 ± 0.10 of baseline, Wilcoxon signed-rank test p = 0.22: post-stim; ctl, 1.48 ± 0.16 of baseline; MEC, 1.31 ± 0.12, Wilcoxon signed-rank test p = 0.56) (Fig 4G-,H-left) but significantly affected NBm-ChAT evoked gamma during the stimulation (n = 6 mice: Slow

Gamma; stim; Ctl, 1.36 ± 0.11, MEC 1.14 ± 0.05 of baseline, Wilcoxon signed-rank test p = 0.03: Fast Gamma; stim; Ctl, 1.25 ± 0.10, MEC 1.11 ± 0.05 of baseline, Wilcoxon signed-rank test p = 0.03) (Fig 4G-,H-middle, right) while having no effect on the 20 Hz responses in the NBm (n = 6 mice; Ctl, 1026.37 ± 340.52 μV^2/Hz; MEC, 902.56 ± 310.82 μV^2/Hz); Wilcoxon signed-rank test, p = 0.06) (Fig 4B). These results indicate that by acting on muscarinic receptors, ACh released from NBm terminals can coordinate ongoing theta activity in BL networks while BL nicotine receptor activation contributes to NBm-ChAT mediated BL rhythmicity in the gamma band.

In contrast to the NBm-BL pathway, CeL responses evoked by PPT-ChAT photo-stimulation were unaffected by ACh receptor antagonism (n = 7 mice: 20 Hz; Ctl, 1.30 ± 0.04; MEC+SCP, 1.26 ± 0.06 of baseline; Wilcoxon signed-rank test, p = 0.57) (Fig S6C-F). These results are consistent with our *in vitro* results demonstrating that PPT-evoked changes in CeL activity were strictly due to the activation of AMPA and NMDA receptors (Fig 3I-N). Worthwhile to note is that despite the lack of cholinergic influence of CeL circuits, i.p. injections of MEC + SCP significantly reduced 20 Hz power locally in the PPT (n=7 mice: Ctl, 880 ± 103 μV^2/Hz; MEC+SCP, 1785 ± 101 μV^2/Hz; Wilcoxon signed-rank test, p = 0.04) (Fig S6B, right) suggesting for activation of a subpopulation of locally acting PPT-ACh neurons or efferent-specific modes of transmission for PPT-ChAT circuits.

Unique ChAT-positive cell populations activate positive and negative reinforcing amygdala pathways in behaving mice

Selective recordings made from CeL and accumbal-projecting BL neurons have demonstrated that they respond preferentially [52] to aversive and appetitive stimuli. These results are in line with circuit mapping studies showing that photo-stimulating BL efferents to the CeL or nucleus accumbens result in defensive [53] and appetitive [53,54] behavioral responding, respectively. Moreover, different amygdala neuronal populations respond to appetitive and aversive stimuli [37,38] but it is unclear which amygdala inputs can communicate such information. We therefore manipulated NBm-BL and PPT-CeL ChAT projections for testing a priori whether these inputs can influence appetitive and/or aversive amygdala pathways. To do so we utilized a conditioned place-preference paradigm where mice were free to explore both regions and photo-activated PPT-CeL or NBm-BL ChAT axons only when mice entered and were within the boundaries of a distinct area of the place preference apparatus (Fig 5A,D). Baseline testing revealed that neither control nor ChR2 mice had a preference for either area of the chamber (Habituation (Hab): GFP (n = 9 mice), 60.2 ± 6.6%; ChR2, (n = 11 mice) 55.6 ± 5.8%) (Fig 5E,F). However, place-specific stimulation resulted in PPT-CeL mice spending less time than GFP-only control mice in the area paired with light stimulation (Conditioning (Cond): GFP, 55.1 ± 7.5%; ChR2, 34.3 ± 6.1%) (Fig 5D,E). Remarkably, after a single conditioning session, mice continued to avoid the stimulation-paired region during a “no-stimulation” test phase

(Testing (Test); GFP 56.4 ± 8.5, ChR2 33.9 ± 5.8%) (Two-Way ANOVA Group F(2,36) = 4.1 p = 0.02; Bonferonni post-hoc test; Hab, Cond, Test - GFP vs ChR2, p = 0.72, p = 0.02, p = 0.01, respectively: Two-Way ANOVA Time F(2,36) = 5.1 p = 0.01; Bonferonni post-hoc test; ChR2, Hab vs Cond p = 0.01; Hab vs Test p = 0.01) (Fig 5D,E). Compared to baseline conditions, during both conditioning and testing phases ChR2 mice spent less time in the stimulation-paired area (Normalized data: Cond/Hab GFP = 1.02 ± 0.13, ChR2 = 0.63 ± 0.12, Unpaired T-Test p = 0.03; Test/Hab GFP = 1.05 ± 0.19, ChR2 = 0.61 ± 0.12, Unpaired T-Test p = 0.043) (Fig 5F). Interestingly, during both conditioning and testing phases, when entering the stimulation-paired area in PPT-CeL ChR2 mice showed a reduction in speed (Two-way ANOVA Group F(1,18) = 7.0 p = 0.01; Bonferonni post-hoc test Hab, Cond, Test – GFP vs ChR2, p = 0.58, p = 0.008, p = 0.02: Time F(2,36) = 25.9; Bonferonni post-hoc test; Control, Hab vs Testing p = 0.009; ChR2, Hab vs. Cond p = 0.0006, Hab vs Test p = 0.0004) (Normalized data in Photostim area: Cond/Hab; GFP 0.93 ± 0.13, ChR2 0.43 ± 0.06, Unpaired T-Test p = 0.01; Test/Hab, GFP 0.71 ± 0.12, ChR2 0.37 ± 0.05, Unpaired T-Test p = 0.03) (Fig S6). As reduced rate of activity is closely associated with defensive behavior in rodent models these results support the premise that exposure to the stimulation-paired area are activating negatively reinforcing CeL pathways.

In contrast, during the conditioning phase photo-activating the NBm-BL pathway led to ChR2 mice spending significantly more time than GFP-only control mice in the light-paired region (habituation: GFP (n = 8 mice), 50.4 ± 8.2%; ChR2 (n = 11 mice), 60.6 ± 6.2%; Two-Way ANOVA Interaction F(2,34) = 4.381 p = 0.02; Bonferonni post-hoc test; GFP vs ChR2, Cond p = 0.03; Hab vs Cond, ChR2 p = 0.008; Cond vs Test p = 0.01) (Fig 5A,B). Compared to baseline conditions, during the conditioning phase mice spent more time in the stimulation-paired area (Normalized data: Cond/Hab GFP = 0.96 ± 0.31, ChR2 = 1.67 ± 0.13, Unpaired T-Test p = 0.04) (Fig 5C-left) but did not continue to prefer the stim-paired area during the testing phase (Normalized data: Test/Hab GFP = 0.92 ± 0.22, ChR2 = 1.26 ± 0.16, Unpaired T-Test p = 0.23) (Fig 5C-right). To further probe the extent by which NBm-BL inputs activate BL reward circuits we paired NBm-BL stimulation with an illuminated touchscreen using a self-stimulation protocol (Fig 5G-I). During conditioning ChR2 and GFP-only mice screen-touched an equal amount. The next day when animals only received stimulation upon correctly touching the paired touchscreen, ChR2 animals performed more correct touches to receive stimulation (Day 1: GFP, 5.5 ± 2.1; ChR2 7.4 ± 1.1; Day 2: GFP, 3.3 ± 0.6; ChR2, 14.5 ± 2.7; Two-way ANOVA Day, F(1,10) = 7.03 p = 0.024, Interaction Day*Group, F(1,10) = 5.5 p = 0.04; Bonferonni post-hoc test Day 2 GFP vs ChR2, p = 0.002, ChR2 Day 1 vs Day 2, p = 0.006) (Fig 5H), supporting the idea that NBm-BL activation of appetitive amygdala pathways can support instrumental learning. This increase in correct touches was likely not due to a general increase in activity as total locomotion, as measured by beam breaks, between the two groups on testing day was not

significantly different (Day 2: GFP, 309.2 ± 42.3; ChR2, 376.3 ± 45.0; Unpaired T-Test t(10) = 0.93, p = 0.37) (Fig 5I).

We next aimed to determine whether NBm- and PPT-ChAT neurons projecting to the BL and CeL, respectively, respond naturally to appetitive and aversive stimuli in wild-type mice (Fig 6). To do so, retrogradely labeling fluorescent latex beads were injected into the BL or CeL. BL-injected mice were subject to a behavioral protocol where, following a food receptacle entry via a nose-poke, had access to a sucrose solution (appetitive) while mice with CeL injections of retrobeads were exposed to mild electrical footshocks (aversive). Two hours following the start of the protocol mice were perfused and brains were processed for visualizing the protein product of the immediate gene cFos – a commonly used molecular marker of neuronal activity - for revealing active BL and CeL projecting NBm- and PPT-ChAT neurons, respectively (Fig 6). Approximately two-thirds of retrogradely labeled NBm-BL and one-half and PPT-CeL neurons were immunopositive for ChAT (n = 8, 6 mice, 656, 395 cells: 64%, 45%, respectively) (Fig 6C,H). Notably, BL and CeL retrobead injections did not retrogradely label cells in the PPT and NBm, respectively, indicating that the population of terminals labeled in the BL and CeL did not originate in the PPT and NBm. Compared to control mice, that received unsweetened drinking water, sucrose-exposed mice had significantly more BL-projecting NBm-ChAT neurons express cFos (Ctl: (n = 5 mice) 10.1 ± 2.1%; sucrose, (n = 5 mice) 23.9 ± 5.4%; Unpaired T-Test, p = 0.04) (Fig 6E). In contrast, when instead of sucrose mice injected with retrobeads in the BL were exposed to unpredicted footshocks there was no difference in cFos expression in BL-projecting Nbm-ChAT neurons (n = 3 mice/condition: Ctl, 2.0 ± 1.1%; footshock, 0.0. ± 0.0%; Unpaired T-Test, p = 0.19) despite expressing defensive behavior (n = 3 mice: Ctl, 8.3 ± 1.1%; footshock, 62.7 ± 3.1%; Unpaired T-Test, p = 0.002) (Fig S7). Surprisingly, few NBm neurons in total were immunopositive for cFos (n = 3 mice/condition: Ctl, 9.0 ± 3.0; footshock, 8.0 ± 2.4). Expanding on previous studies [28-31], these results demonstrate that a subpopulation of NBm neurons responding to appetitive stimuli project to the BL. In CeL injected mice, we did not observe any difference in cFos expression in PPT-ChAT neurons between control mice and those that had received footshocks (Ctl, 1.5 ± 0.9%; footshock, 1.0 ± 0.9%; n = 4 mice per group, Unpaired T-Test, p = 0.71) (Fig 6J). However, consistent with previous research [55], the scarcity of cFos expressing PPT-ChAT neurons makes this data difficult to interpret.

Discussion:

Our results reveal that input-specific cholinergic projections to different amygdala nuclei can differentially affect amygdala circuits through unique modes of communication engaging both cellular and network-level processes that are known to support learning-related plasticity. Consistent with this, photo-activating NBm-BL and PPT-CeL pathways induced behavioral changes by influencing

amygdala circuits involved in approach and avoidance behavior, respectively. Taken together, these results reveal distinct cholinergic influences on amygdala circuits and motivational behavior.

Principal amygdala neurons are synaptically influenced by both fast and slow cholinergic transmission

Recent experimental evidence supports a mode of central cholinergic transmission that is both synaptic [56] and via volume transmission [57]. Consistent with previous work [45], NBm terminals were seen to reliably inhibit a high percentage of BL neurons and the current data indicates that this inhibition is due to a M1 receptor-dependent increase in GIRK channel conductance. Anatomical work has demonstrated the existence of both synaptic and extra-synaptic M1 receptors [58,59]. In line with these morphological observations, the physostigmine-sensitive inhibitory responses measured in the current study were likely caused by the reliable release of endogenous ACh acting at or near the synapse to increase K^+ conductance. In contrast, the slow M1-mediated excitation resulting from high frequency stimulation may result from a separate class of extra-synaptic M1-receptors that are coupled to M1-mediated decreases in K^+ conductance [60]. Taken together, these results provide support for both synaptic and volume ACh transmission via separate M1-mediated mechanisms for coordinating ongoing BL activity. Although the M1 inhibitory response is likely due to ACh terminals in close proximity to BL principal neurons, whether or not the relatively slower depolarizing M1 effects are mediated via the same neurons or through nonspecific increases in ACh arising from the dense axonal arborization of NBm-ACh to BL inputs (Fig 1B,C) is currently unknown and of interest for future work.

Rhythmic coordination of amygdala activity by NBm cholinergic populations

In many instances these M1-mediated responses resulted in a biphasic inhibition-excitation profile in BL principal neurons. When NBm-ChAT inputs to the BL were similarly stimulated at 20 Hz *in vivo*, the theta and low gamma power of NBm and BL population activity was significantly increased. Our results further show that increased synchrony in the theta band that outlasted NBm-ChAT stimulation was dependent of muscarinic receptor activation, revealing a direct influence of NBm-ChAT terminals on coordinating BL principal neuron activity. Moreover, nicotinic receptor activation contributed to NBm-evoked gamma oscillations in the BL specifically during stimulation. In addition to influencing principal neurons, NBm-ChAT projections to the BL have been shown to depolarize late-spiking (LTS) interneurons that can regulate the activity of BL principal neurons [45]. Through a combination of a direct muscarinic inhibition-excitation and indirect inhibition, via nicotinic receptor-mediated activation of LTS interneurons onto principal neurons, these results indicate that an interplay between both receptor types acting on different BL cell populations can effectively synchronize BL networks. Cholinergic circuits have been shown to promote neural oscillations in efferent regions [19-21] and

behaviorally, amygdala oscillations in the theta and gamma frequency band have been linked to learned [43,44] and innate emotional responses [41,42]. Interestingly, in the latter case, coherent prefrontal-amygdala activity is strongly related with fear or safety signaling [41,42]. As the NBm can synchronize amygdala and prefrontal [61,62] activity our results raise the possibility that such behaviorally-relevant increases in PFC-amygdala coherence may in part stem from coordinated NBm activity that influences both structures.

Brainstem ChAT neurons act to excite CeL amygdala circuits by releasing glutamate that synergistically activates AMPA and NMDA receptors

In the current investigation, CeL responses to PPT-ChAT stimulation *in vivo* were insensitive to ACh antagonists. Interrogation of this circuit *ex vivo* revealed that PPT-ChAT mediated responses were due to a glutamatergic excitation, where early and late depolarizing components were due to AMPA and NMDA receptor activation, respectively. Glutamatergic transmission by cholinergic neurons is not unusual as prior studies have shown that glutamate release from cholinergic neurons can effectively impact postsynaptic targets [50,56]. Consistent with this, PPT ChAT-expressing neurons have been shown to express synaptic glutamate markers [49]. Despite robust expression of ChR2 in PPT-ChAT neurons (Fig 1E,F; S1E,F), many of which projecting to the CeL (Fig 6G,H), neither exogenously applied ACh nor the stimulation parameters used here evoked a cholinergic receptor-dependent response on CeL neurons, suggesting that the predominant impact of PPT-ChAT terminals in the CeL is via the release of glutamate. In light of our results, it is plausible that a locally-acting population of PPT-ChAT neurons via cholinergic transmission are influencing PPT activity. Alternatively, that glutamate and ACh release from CeL-projecting PPT-ChAT neurons follow a similar domain-specific transmission mechanism as a subpopulation of dopamine neurons where glutamate and dopamine from the same axon are released from distinct terminal sites [63].

NMDA receptor activation in response to PPT terminal stimulation led to a sustained increase in excitability only at membrane potentials close to threshold suggesting that PPT inputs are most effective at sustaining CeL activity at depolarized levels. It is well established that by acting as activity-based coincidence detectors, NMDA receptors are critical for synaptic plasticity that underlies learning and memory. NMDA currents in CeL neurons have been shown to increase in amplitude following fear conditioning [64] and blocking them reduce both auditory and contextual fear conditioning [65], demonstrating a functional role for these receptors in fear learning. Interestingly, the response kinetics of CeL neurons are known to be relatively slow compared to those in BL principal neurons [66]. It is thus conceivable that, by activating NMDA receptors on CeL neurons, PPT-CeL inputs would lead to a larger calcium permeability and longer period of synaptic integration onto CeL neurons, providing a

synaptic mechanism whereby PPT-ChAT inputs to the CeL can support plasticity and as a consequence emotional memory formation [64,65].

***In vivo* photo-activation of BL and CeL inputs from distinct ChAT cell populations drives opposing approach and avoidance learning-related changes in behaving mice**

Our behavioral data indicates that activating NBm versus PPT ACh-neurons can reinforce behavior by respectively biasing amygdala processing towards approach and avoidance behavior. These results point towards an input- and nucleus-specific complementary role of distinct cholinergic influences on amygdala functions. It is conceivable that PPT-CeL inputs preferentially contact CeL microcircuits important for fear learning instead of CeL neurons important for appetitive emotional processes [67]. Notable are our findings that approximately 70% of PPT-ChAT connected CeL neurons showed signature late-spiking properties while the rest were of the regular spiking variety. In seeming contrast to our data, PKCδ^+ CeL neurons identified as late-spiking have been shown to be important in reducing the expression of defensive behavior [68]. Li et al., [64] however have shown that somatostatin (SOM)-expressing CeL neurons important for fear memory and expression also show late-spiking as well as regular-spiking properties. Interestingly, in the same study, fear conditioning led to an increase in CeL SOM$^+$ excitability that when disrupted reduced fear learning, indicating that the contribution of this mixed population of CeL neurons to fear learning and expression is dependent on synaptic changes in their excitability. As late-spiking neurons make up a third of CeL neurons [66] it is likely that multiple classes exist for differently regulating fear-related processes.

Cholinergic inputs to the basolateral division on the amygdala drive reward-based learning

Contrary to PPT inputs to the ventral tegmental area known to support appetitive learning [69] the above behavioral findings indicate that PPT inputs to the CeL, can induce long-term changes in circuits that mediate avoidance behavior. Our conditioned place preference, self-stimulation, and cFos tracing results in contrast indicate that NBm-ChAT inputs to the BL respond to appetitive stimuli and activate BL circuits that support approach behavior, a result consistent with previous work demonstrating that BL specific inputs to the NAc can similarly reinforce appetitive behavior [54]. Moreover, NBm-ChAT neurons projecting to the BL did not increase their responses to unsignaled aversive stimuli as indicated by cFos expression measurements. These results differ to a recent paper showing that NBm-BL activation can support fear learning [46]. This seeming contradiction may arise from the fact that in the Jiang et al. study NBm-BL axons were photo-stimulated during tone-shock pairings thereby influencing robust naturally occurring co-activated amygdala inputs. In the current study, NBm fibers were activated only when mice freely explored a neutral context or when contacting a neutral stimulus (touchscreen).

One notable anatomical observation was that NBm ACh axons strongly innervated the BL while the lateral amygdala (LA) was almost entirely devoid of such fibers. Neurons within the BL respond to stimuli with positive and negative valence [37,38]. It is thus hard to reconcile how such an influential ACh input can preferentially contact neurons that make up appetitive amygdala circuits. The rostral-caudal position alone cannot fully explain these findings since we positioned the fiber optic implants at 1.5 mm caudal from bregma where both positive and negative valence-coding neurons reside [70]. The highly segregated NBm-ChAT projection to the BL however allowed us to pinpoint the specific influences of ACh populations on BL function that was independent of the LA. Despite much experimental evidence demonstrating that LA and BL neurons respond to both positive and negative valence stimuli, data exists to support the idea that the LA and BL may in some instances be performing non-overlapping functions. For example, lesions restricted to the LA impair fear conditioning while BL selective lesions do not [71,72]. Moreover, LA neurons undergo fear-related plasticity [43,73] and activating LA populations can support fear memory [74] while BL neurons can also respond to safety signals [75] and their activation can facilitate reward seeking [54]. Interestingly, recent work by Lee et al. [76] has shown that increases in BL neuronal activity correspond more with the behavioral output of the reward-seeking response than to the stimulus driving the response, irrespective of the behavioral output being conditioned or spontaneous. This data suggests that specific BL circuits, rather than mostly communicating sensory-related information, are wired for generating appropriate motivation-based behavior.

Our results show that coordinating BL activity with NBm-ChAT activation increases exploration in the stimulation-paired region as well as operant responding in a self-stimulation paradigm. Moreover, BL-projecting ChAT neurons increase their activity with exposure to appetitive but not unsignaled aversive stimuli as measured with the molecular activity marker cFos. Operant approach and avoidance behavior has been shown to rely on an intact BL that together with the current data illustrate that specific inputs to this region can facilitate operant approach and touchscreen responding. Since NBm neurons rapidly respond to natural and learned emotionally-salient stimuli [28-31] it is possible that salient information is relayed to the amygdala through ACh neurons, thereby contributing to BL valence coding that can ultimately support BL-dependent plasticity and learning and memory. In line with this idea, pairing an auditory stimulus with NBm-stimulation can result in associative memory [77] and recent work by Jiang et al. [46] has shown that stimulation of NBm-BL inputs is sufficient to induce long-term potentiation of synaptic responses in the BL. Collectively, these results support the idea that by way of coordinating network activity, NBm-ChAT inputs to the BL may be providing the physiological substrate necessary for salience detection and attention that are important for learning and memory. Although the data presented here demonstrates that BL-projecting NBm-ChAT neurons respond to appetitive stimuli and drive positive reinforcement, future studies that

measure appetitive or aversive emotional memory following inactivation of NBm-BL pathways would help elucidate the significance of NBm influences on amygdala-dependent learning and memory.

In summary, our results reveal complementary anatomical, synaptic, and behavioral cholinergic influences on amygdala microcircuits. As cholinergic neurons and amygdala function are critical for emotional learning and memory our results demonstrate distinct mechanisms through which central ACh populations can engage processes known to promote associative biophysical changes that underlie emotional memories. By doing so these results advance our understanding of the underlying neural mechanisms supporting emotional learning and consequently those affected in diseases such as Alzheimer's Disease, where severe disruptions in central cholinergic systems result in disabling impairments in emotional memories.

Acknowledgements:

This work was supported by the Royal Society, The Wellcome Trust (JAS), the Sigrid Juselius Foundation (TA), and by a Herchel Smith Fellowship (YAH).

Author Contribution:

Conceptualization, T.A., Y.A.H., B.U.P., J.A-S.; Methodology, T.A., Y.A.H., B.U.P., J.A-S.; Formal Analysis, T.A., Y.A.H., B.U.P., J.A-S.; Investigation, T.A., Y.A.H., B.U.P., J.A-S.; Resources, L.M.S, T.J.B., O.P., J.A-S.; Writing – Original Draft, J.A-S. Writing – Review and Editing, T.A., Y.A.H., B.U.P., T.J.B., O.P., J.A-S.; Visualization, T.A., Y.A.H., J.A-S.; Supervision, J.A-S., Project Administration, J.A-S.; Funding Acquisition, L.M.S, T.J.B., O.P., J.A-S.

Declaration of Interests:

The authors declare no competing interests

References:

1. Underwood, G. Attention and Memory. Elsevier (2013).

2. Corbetta, M., and Shulman, G.L. (2002). Control of goal-directed and stimulus-driven attention in

3. Klinkenberg, I., Sambeth, A. and Blokland, A. (2011). Acetylcholine and attention. Behavioural Brain Research, 221, 430–442.

4. Paolone, G., Angelakos, C.C., Meyer, P.J., Robinson, T.E. and Sarter, M. (2013). Cholinergic control over attention in rats prone to attribute incentive salience to reward cues. Journal of Neuroscience 33, 8321-8335.

5. Holland, P.C. and Gallagher, M. Amygdala circuitry in attentional and representational processes. Trends in Cognitive Sciences 3, 65–73 (1999).

6. Williams, M.A., McGlone, F., Abbott, D.F. and Mattingley, J.B. (2005). Differential amygdala responses to happy and fearful facial expressions depend on selective attention. Neuroimage 24, 417-425.

7. Hasselmo, M.E. (2006). The role of acetylcholine in learning and memory. Current Opinion in Neurobiology, 16, 710–715.

8. Herry, C., et al. (2007). Processing of temporal unpredictability in human and animal amygdala. Journal of Neuroscience 27, 5958-5966.

9. Roesch, M.R., Calu, D.J., Esber, G.R. and Schoenbaum, G. (2010). Neural correlates of variations in event processing during learning in basolateral amygdala. Journal of Neuroscience 30, 2464-2471.

10. Perry R.J. and Hodges J.R. (1999). Attention and executive deficits in Alzheimer's disease: A critical review. Brain 122, 383-404.

11. Mori, E., et al. (1999). Amygdalar volume and emotional memory in Alzheimer’s disease. American Journal of Psychiatry 156, 216-222.

12. Kensinger, E.A., Brierley, B., Medford, N., Growdon, J.H. and Corkin, S. (2002). Effects of normal aging and Alzheimer's disease on emotional memory. Emotion 2, 118.

13. Herholz, K., et al. (2004). In vivo study of acetylcholine esterase in basal forebrain, amygdala, and cortex in mild to moderate Alzheimer disease. Neuroimage, 21, 136-143.

14. Poulin, S.P., et al. (2011). Amygdala atrophy is prominent in early Alzheimer's disease and relates to symptom severity. Psychiatry Research: Neuroimaging, 194(1), pp.7-13.

15. Gill, T.M., Sarter, M. and Givens, B. (2000). Sustained visual attention performance-associated prefrontal neuronal activity: evidence for cholinergic modulation. The Journal of Neuroscience 20, 4745–4757.

16. Disney, A.A., Aoki, C. and Hawken, M.J. (2007). Gain modulation by nicotine in macaque v1. Neuron, 56, 701–713.

17. Ma, M, and Luo, M. (2012). Optogenetic activation of basal forebrain cholinergic neurons modulates neuronal excitability and sensory responses in the main olfactory bulb. Journal of Neuroscience 25, 10105-10116.

18. Pinto, L., et al. (2013). Fast modulation of visual perception by basal forebrain cholinergic neurons. Nature Neuroscience 16, 1857-1863.

19. Metherate, R., Cox, C.L. and Ashe, J.H. (1992). Cellular bases of neocortical activation: modulation of neural oscillations by the nucleus basalis and endogenous acetylcholine. The Journal of Neuroscience 12, 4701–4711.

20. Fisahn, A., Pike, F.G., Buhl, E.H. and Paulsen, O. (1998). Cholinergic induction of network oscillations at 40 Hz in the hippocampus in vitro. Nature 394, 186.

21. Vandecasteele, M., et al. (2014). Optogenetic activation of septal cholinergic neurons suppresses sharp wave ripples and enhances theta oscillations in the hippocampus. Proceedings of the National Academy of Sciences 111, 13535-13540.

22. Börgers, C., Epstein, S. and Kopell, N.J. Background gamma rhythmicity and attention in cortical local circuits: a computational study. Proceedings of the National Academy of Sciences 102, 7002–7007 (2005).

23. Bauer M., Stenner M.P., Friston K.J., and Dolan R.J. (2014). Attentional modulation of alpha/beta and gamma oscillations reflect functionally distinct processes. Journal of Neuroscience. 34, 16117-25.

24. Gu, Z. and Yakel, J.L. (2011). Timing-dependent septal cholinergic induction of dynamic hippocampal synaptic plasticity. Neuron 71, 55–165.

25. Brzosko, Z., Zannone, S., Schultz, W., Clopath, C. and Paulsen, O. (2017). Sequential neuromodulation of Hebbian plasticity offers mechanism for effective reward-based navigation. eLife 6.

26. Jones, B.E. From waking to sleeping: neuronal and chemical substrates. (2005). Trends in Pharmacological Sciences 26, 578–586.

27. Dautan D., et al. (2016). Segregated cholinergic transmission modulates dopamine neurons integrated in distinct functional circuits. Nature Neuroscience 19, 1025-33.

28. Richardson, R.T. and DeLong, M.R. (1986). Nucleus basalis of Meynert neuronal activity during a delayed response task in monkey. Brain Research 399, 364–368.

29. Wilson, F.A.W. and Rolls, E.T. (1990) Neuronal responses related to reinforcement in the primate basal forebrain. Brain research 509, 213–231.

30. Lin, S.C. and Nicolelis, M.A. (2008) Neuronal ensemble bursting in the basal forebrain encodes salience irrespective of valence. Neuron 59, 138-149.

31. Hangya, B., Ranade, S.P., Lorenc, M. and Kepecs, A. (2015). Central cholinergic neurons are rapidly recruited by reinforcement feedback. Cell 162, 1155-1168.

32. Okada, K., Toyama, K., Inoue, Y., Isa, T., and Kobayashi, Y. (2009). Different pedunculopontine tegmental neurons signal predicted and actual task rewards. Journal of Neuroscience. 29, 4858-4870.

33. Grove, E.A. (1988). Efferent connections of the substantia innominata in the rat. Journal of Comparative Neurology 277, 347–364.

34. Woolf, N.J. and Butcher, L.L. (1982). Cholinergic projections to the basolateral amygdala: a combined Evans Blue and acetylcholinesterase analysis. Brain Research Bulletin 8, 751–763.

35. Hallanger, A.E. and Wainer, B.H. (1988). Ascending projections from the pedunculopontine tegmental nucleus and the adjacent mesopontine tegmentum in the rat. Journal of Comparative Neurology 274, 483–515.

36. Janak, P.H. and Tye, K.M. (2015). From circuits to behaviour in the amygdala. Nature, 517(7534), pp.284–292.

37. Nishijo, H., Ono, T. and Nishino, H. (1988). Single neuron responses in amygdala of alert monkey during complex sensory stimulation with affective significance. The Journal of neuroscience 8, 3570–3583.

38. Paton, J.J., Belova, M.A., Morrison, S.E. and Salzman, C.D. (2006). The primate amygdala represents the positive and negative value of visual stimuli during learning. Nature 439, 865.

39. Saddoris, M.P., Gallagher, M. and Schoenbaum, G. (2005). Rapid associative encoding in basolateral amygdala depends on connections with orbitofrontal cortex. Neuron 46, 321–331.

40. Inglis WL, Olmstead MC, Robbins TW. (2000). Pedunculopontine tegmental nucleus lesions impair stimulus–reward learning in autoshaping and conditioned reinforcement paradigms. Behavioral Neuroscience 114, 285–294.

41. Likhtik, E., Stujenske, J.M., Topiwala, M.A., Harris, A.Z. and Gordon, J.A. (2014). Prefrontal entrainment of amygdala activity signals safety in learned fear and innate anxiety. Nature Neuroscience 17, 106-113.

42. Stujenske, J.M., Likhtik, E., Topiwala, M.A. and Gordon, J.A. (2014). Fear and safety engage competing patterns of theta-gamma coupling in the basolateral amygdala. Neuron 83, 919-933.

43. Paré, D. and Collins, D.R. (2000). Neuronal correlates of fear in the lateral amygdala: multiple extracellular recordings in conscious cats. The Journal of Neuroscience 20, 2701–2710.

44. Popescu, A.T., Popa, D. and Paré, D. Coherent gamma oscillations couple the amygdala and striatum during learning. Nature Neuroscience 12, 801–807 (2009).

45. Unal, C.T., Paré, D. and Zaborszky, L. (2015). Impact of basal forebrain cholinergic inputs on basolateral amygdala neurons. The Journal of Neuroscience 35, 853–863.

46. Jiang, L., et al. (2016). Cholinergic signaling controls conditioned fear behaviors and enhances plasticity of cortical-amygdala circuits. Neuron 90, 1057-1070.

47. Gulledge, A.T. and Stuart, G.J. (2005). Cholinergic inhibition of neocortical pyramidal neurons. Journal of Neuroscience 25, 10308-10320.

48. Power, J.M. and Sah, P. (2008). Competition between calcium-activated K+ channels determines cholinergic action on firing properties of basolateral amygdala projection neurons. Journal of Neuroscience 28, 3209-3220.

49. Lavoie, B. and Parent, A. (1994). Pedunculopontine nucleus in the squirrel monkey: cholinergic and glutamatergic projections to the substantia nigra. Journal of Comparative Neurology 344, 232–241.

50. Gras, C., et al. The vesicular glutamate transporter VGLUT3 synergizes striatal acetylcholine tone. Nature Neuroscience 11, 292-300 (2008).

51. Datta, S. and Siwek, D.F. (2002). Single cell activity patterns of pedunculopontine tegmentum neurons across the sleep- wake cycle in the freely moving rats. Journal of neuroscience research 70, 611–621.

52. Beyeler, A., et al. (2016). Divergent routing of positive and negative information from the amygdala during memory retrieval. Neuron 90, 348-361.

53. Namburi, P., et al. (2015). A circuit mechanism for differentiating positive and negative associations. Nature 520, 675.

54. Stuber, G.D., et al. (2011). Excitatory transmission from the amygdala to nucleus accumbens facilitates reward seeking. Nature 475, 377-380.

55. Nakahara, D., Ishida, Y., Nakamura, M., Furuno, N. and Nishimori, T. (2001). Intracranial self-stimulation induces Fos expression in GABAergic neurons in the rat mesopontine tegmentum. Neuroscience 106, 633-641.

56. Hay, Y.A., Lambolez, B. and Tricoire, L. (2015). Nicotinic transmission onto layer 6 cortical neurons relies on synaptic activation of non-α7 receptors. Cerebral Cortex 26, 2549-2562.

57. Yamasaki, M., Matsui, M. and Watanabe, M. (2010). Preferential localization of muscarinic M1 receptor on dendritic shaft and spine of cortical pyramidal cells and its anatomical evidence for volume transmission. Journal of Neuroscience 30, 4408-4418.

58. Muller, J.F., Mascagni, F., and McDonald, A.J. (2011). Cholinergic innervation of pyramidal cells and parvalbumin-immunoreactive interneurons in the rat basolateral amygdala. Journal of Comparative Neurology 519, 790–805.

59. Muller, J.F., Mascagni, F., Zaric, V., McDonald, A.J. (2013). Muscarinic cholinergic receptor M1 in the rat basolateral amygdala: ultrastructural localization and synaptic relationships to cholinergic axons. Journal of Comparative Neurology 521, 1743–1759.

60. Faber, E.S.L. and Sah, P. (2002). Physiological role of calcium-activated potassium currents in the rat lateral amygdala. The Journal of Neuroscience 22, 1618–1628.

61. Nguyen, D.P. and Lin, S.C. (2014). A frontal cortex event-related potential driven by the basal forebrain. Elife 3, p.e02148.

62. Kim, T., et al. (2015). Cortically projecting basal forebrain parvalbumin neurons regulate cortical gamma band oscillations. Proceedings of the National Academy of Sciences 112, 3535-3540.

63. Zhang, S., et al. (2015). Dopaminergic and glutamatergic microdomains in a subset of rodent mesoaccumbens axons. Nature Neuroscience, 18 386-392.

64. Li H,. et al. (2013). Experience-dependent modification of a central amygdala fear circuit. Nature Neuroscience 16, 332–339.

65. Goosens, K.A. and Maren, S. (2003). Pretraining NMDA receptor blockade in the basolateral complex, but not the central nucleus, of the amygdala prevents savings of the conditional fear. Behavioral Neuroscience 117, 738.

66. de Armentia, M.L. and Sah, P. (2003). Development and subunit composition of synaptic NMDA receptors in the amygdala: NR2B synapses in the adult central amygdala. Journal of Neuroscience 23, 6876-6883.

67. Tye K.M., et al. (2011). Amygdala circuitry mediating reversible and bidirectional control of anxiety. Nature 471, 358–362.

68. Haubensak, et al. (2010). Genetic dissection of an amygdala microcircuit that gates conditioned fear. Nature 468, 270-276.

69. Yau, H.J., et al. (2016). Pontomesencephalic tegmental afferents to VTA non-dopamine neurons are necessary for appetitive Pavlovian learning. Cell reports 16, 2699-2710.

70. Kim, J., Pignatelli, M., Xu, S., Itohara, S. and Tonegawa, S. (2016). Antagonistic negative and positive neurons of the basolateral amygdala. Nature Neuroscience 19, 1636-1646.

71. Amorapanth, P., LeDoux, J.E. and Nader, K. (2000). Different lateral amygdala outputs mediate reactions and actions elicited by a fear-arousing stimulus. Nature neuroscience 3, 74-79.

72. Nader, K., Majidishad, P., Amorapanth, P. and LeDoux, J.E. (2001). Damage to the lateral and central, but not other, amygdaloid nuclei prevents the acquisition of auditory fear conditioning. Learning and Memory 8, 156-163.

73. Quirk, G.J., Repa, J.C. and LeDoux, J.E. (1995). Fear conditioning enhances short-latency auditory responses of lateral amygdala neurons: parallel recordings in the freely behaving rat. Neuron 15, 1029–1039.

74. Johansen, J.P., et al. (2010). Optical activation of lateral amygdala pyramidal cells instructs associative fear learning. Proceedings of the National Academy of Sciences 107, 12692-12697.

75. Sangha, S., Chadick, J.Z. and Janak, P.H. Safety encoding in the basal amygdala. Journal of Neuroscience 33, 3744-3751 (2013).

76. Lee, S.C., Amir, A., Headley, D.B., Haufler, D. and Pare, D. (2016). Basolateral amygdala nucleus responses to appetitive conditioned stimuli correlate with variations in conditioned behaviour. Nature communications 7.

77. McLin III, D.E., Miasnikov, A.A. and Weinberger, N.M. (2002). The effects of electrical stimulation of the nucleus basalis on the electroencephalogram, heart rate, and respiration. Behavioral Neuroscience 116, 795.

MATERIALS AND METHODS

Animal procedures followed United Kingdom Home Office regulations.

Experimental animals

Male heterozygous mice expressing Cre recombinase under the control of the ChAT promoter [ChAT-cre mice (B6N;129S6-Chattm2(cre)Lowl/J), The Jackson Laboratory, Bar Harbor, ME, USA] were used in the experiments. Mice were housed 2-10 animals per polycarbonate cage and provided ad libitum with water and standard lab chow (RM3, Special Diet Services, Essex, UK) in a holding room maintained under 12-h light cycle (lights off at 7 p.m.) with temperature regulated at 22-24°C and relative humidity kept at 50-55%. Mice were genotyped using PCR from ear notch biopsy. Before commencing behavioural testing the animals were handled daily for one week, and 1 h before each behavioural trial the mice were transported to the respective testing area. The experiments were performed during the light phase of the light/dark cycle. All animal care and experimental procedures were conducted in accordance with the UK Animals (Scientific Procedures) Act, 1986.

Neurosurgery, Viral Transfection and Fiber Optic Implants

ChAT:cre mice at the age of 2.5 months were anaesthetized with isoflurane (5% induction, 1-2% maintenance, Abbott Ltd, Maidenhead, UK) mixed with oxygen as a carrier gas (flow rate 0.8-1.0 L/min), placed in a stereotactic frame (David Kopf Instruments, Tujunga, CA, USA), the skull exposed via a small incision, and a small bilateral craniotomy was performed to allow intracranial injections and placement of fiber optic implants. A stainless steel bevelled microinjector was lowered to a coordinate aimed at the basal forebrain (anteroposterior +0.05 mm in relation to bregma, laterally +/- 1.15 mm in relation to midline and at –5.0 mm from the skull level) and brain stem PPT (anteroposterior -4.60 mm in relation to bregma, laterally +/- 1.00 mm in relation to midline and at –3.50 mm from the skull level). Microinjector was connected to a 1 µL Hamilton glass syringe via polyethylene tubing and injection rate of 0.1 µL/min was regulated by a microprocessor controlled programmable syringe pump (KD Scientific Inc., Holliston, MA, USA). Injection site received 200 nL volume of one of the following viruses: AAV5-EF1α-DIO-GFP or AAV5-EF1α-DIO-hChR2(H134R)-GFP, (titer $4x10^{12}$ vg/mL, University of North Carolina, Gene Therapy Center, NC, USA) followed by 5-min wait. For postoperative care mice received meloxicam (1 mg/kg. s.c., Boehringer Ingelheim Ltd. Bracknell, UK) and a recovery period of 4 weeks was attained before commencing fiber optic implantation.

For behavioural experiments, chronic fiber optic implants were fabricated by connecting stripped optic fiber (200 µm, FT200EMT 0.39NA, Thorlabs, Newton, NJ, USA) to ferrules (CFLC230,Thorlabs) as reported previously (Sparta et al. 2012, Nat Protocols 7:12-23). Using the same inhalation anaesthesia protocol as for viral transduction and surgical preparation, the skull was exposed and fiber optic implants were lowered to a coordinate at the basolateral amygdala for the basal forebrain injected animals (anteroposterior -1.50 mm in relation to bregma, laterally +/- 2.70 mm in relation to midline and at –4.00 mm from the skull level) or central lateral amygdala for the PPT injected animals (anteroposterior -1.20 mm in relation to bregma, laterally +/- 2.30 mm in relation to midline and at –4.40 mm from the skull level). Fiber optic implants were attached to the skull using two miniature screws and dental cement. Meloxicam (2 mg/kg s.c.) was administered as analgesia and animals were let recover in a postoperational chamber with maintained +36.0°C.

Electrophysiology and in vitro photostimulation

Coronal slices were made >9 weeks post-injection as in our previous study. 250 mm thick slices were cut with a Leica VT 1200S vibratome in ice-cold ACSF (see below), and allowed to recover for 1 hour at 35 °C in ACSF before recordings. Patch pipettes were manufactured from borosilicate glass, and their tip resistances were 4-6 MΩ when filled with K-gluconate solution (see below). Whole-cell recordings were carried out at 37 °C using an EPC-10 amplifier and PatchMaster software (HEKA Elektronik, Germany). Only cells with access resistances of <20 MΩ were used for analysis. Current

signals were low-pass filtered at 3 kHz and digitized at 10 kHz. Data were analyzed with Minianalysis (Synaptosoft), Igor and Adobe Illustrator/ Photoshop. Whole-cell recordings were performed at 35°C using an EPC-10 amplifier and Patch-Master software (HEKA Elektronik). ChAT-containing cells were visualized in acute living brain slices using a GFP filter set (Chroma). To stimulate ChR2, we used a ThorLabs blue LED, delivering ~10 mW/mm2 light to ChR2-containing axons around the recorded cell 40x 0.8NA objective.

Chemicals and solutions:
Slice-cutting and recording ACSF was gassed with 95% O2 and 5% CO2, and contained the following (mM): NaCl 125, $NaHCO_3$ 25, KCl 3, NaH_2PO_4 1.25, $CaCl_2$ 1/2 (cutting/recording), $MgCl_2$ 6/1 (cutting/recording), sodium pyruvate 3 and glucose 25/5 (cutting/recording). Pipettes were filled with (in mM): potassium gluconate 135, NaCl 7, Hepes 10, Na_2-ATP 2, Na-GTP 0.3, and $MgCl_2$ 2; pH was adjusted to 7.3 with KOH. All chemicals were from Sigma, Tocris, and Abcam.

Behavioral Assays

Animals: All animals were initially weighed for 3 consecutive days to establish free-fed weights. Weights were then restricted to approximately 85% of their free-fed weight via daily provision of standard laboratory chow. Water was available ab libitum throughout the study. Animals were kept under a 24h light/dark cycle (lights on 0700, lights off 1900). All behavioral testing was carried out under the light cycle. Prior to behavioral testing, animals were removed from the home-room and taken to the testing room. Following completion of daily testing, animals were returned to the home-room.

Place conditioning:
Behavioral tests were started by habituating animals to the connecting of laser patch cables with the fiber optic implants. The conditioning apparatus consisted of a chamber (45 x 23 x 20 cm) with two distinct equal sized contextual zones that differed in their tactile floor surface (mesh and smooth). There was no wall or door between the zones and animals were thus free to move between the contextual spaces. The location and movement data were collected by video tracking using Ethovision XT software (Noldus Information Technology bv, Wageningen, The Netherlands). On day one, in a habituation test, animals were connected to the laser patch cables and let freely explore the chamber without laser stimulation. On day two in a 15-min conditioning trial, laser stimulation was delivered every time the animal was in the stimulation-paired zone, and the stimulation was not delivered when the animal was in the non-stimulation zone. On the day three in a 15-min testing trial, the animals were again connect to the laser, placed in the chamber with the floors, and let freely move in the chamber without laser stimulation. The laser stimulation-floor type pairing and the orientation (left-right) of the floor materials in the chamber were counterbalanced within the experimental groups.

Self-Stimulation:
Apparatus:
The Bussey-Saksida touchscreen chamber, a trapezoidal operant chamber, is contained within a sound-attenuating box. One end of the chamber is comprised of a touchscreen. Reponses are registered by breaking a set of infra-red beams located less than 5mm from the surface of the screen. At the other end of the chamber a small aperture standardly delivers liquid reinforcer. This was blocked by a metal plate throughout the duration of this study. Throughout testing, a standard '5-choice' Perspex mask, which comprises 5 evenly spaced apertures, was placed in front of the touchscreen to focus responses and protect the edges of the screen. Two sets of infrared beams (at the front and back of the box) were used for measurement of locomotor activity and initiation of task events.

Protocol:
On the first day of testing, all animals were placed on an 'initial touch' schedule to establish an

association between the central stimulus and stimulation. Under this schedule, the central location of the 5-choice mask was illuminated by a white square stimulus for 30 seconds. Following this, the illumination ceased and the animal immediately received stimulation for 10s. If the illuminated location was touched during the 30s window, the illumination immediately ceased and the animal received 30s of stimulation. A front beam break was required to initiate the next trial. These sessions terminated after either 30 successfully completed trials or 60 minutes. On the second day of testing, stimulation was controlled by a fixed ratio 1 schedule (FR1), which required animals to make a single touch at the center location for 10s of stimulation. Illumination at the central stimulus ceased when the stimulus was touched. A new trial was initiated by breaking the front beam. The center location was illuminated until a successful center touch was made. This session was terminated following either completion of 30 trials or after 60 minutes had elapsed. Following completion of behavioural tests, measures for trials completed, blank touches, and front and back beam breaks were extracted from Abet Touch II testing software and analyzed.

Sucrose delivery:

After recovery mice were habituated to the operant chambers residing in sound-attenuating boxes (Med Associates, Fairfax, USA, operated by K-Limbic software, Conclusive Solutions, Sawbridgeworth, UK) for 3 consecutive days. For the sucrose delivery, the chambers were equipped with a food receptacle consisting a photobeam for detection of mouse nose-pokes. A nose-poke triggered a random (interval 3-17 s.) latency for delivery of a liquid sucrose reinforcer (15% w/v sucrose solution in water). Mice were given 90 min to consume sucrose, while for the control animals the reinforcer was not delivered. Immediately after the trial the mice were perfusion fixed as described above.

Foot shock delivery:

After recovery mice were habituated to the fear conditioning chambers residing in sound-attenuating boxes (Med Associates, Fairfax, USA) for 3 consecutive days. For the foot shock delivery, mice received foot shock (1.2 mA, 2 s) on a pseudorandom interval (range 1-7 min) over a 30 min trial. For the control animals no foot shocks were delivered. The mice were returned to their home cages and 60 min afterwards perfusion fixed as described above.

Optical stimulation in vivo

Laser light was generated by using 473-nm diode laser (Versalase, Vortran Laser Technology Inc., Sacramento, CA, USA) controlled by Arduino Uno microcontroller (Arduino Community) to generate pulsing (20 Hz, 5 ms pulse length) with ~15 mW laser power at the tip of the fiber optic implant. Prior to surgical implantation the implants were tested and accepted for implantation with laser light transmittance rate of 75-85% of power measured from patch cable output.

Acute in vivo recordings

Procedure:

Adult mice ChAT-Cre*Ai32 or ChAT-CRE injected with AAV5-EF1a-ChR2-eYFP at least 8 weeks prior to recordings. Mice were deeply anesthetized via intraperitoneal injections of urethane (1.5 to 1.8 g/kg injected in several shots until loss of reflexes is assessed by paw pinching). While restrained in a stereotaxic apparatus (David Kopf instruments, Phymep, France) their temperature was monitored and maintained at 34-36° C using a heating blanket (Basi). After exposing the skull two small burr hole were drilled at NBm coordinates AP = +0.3 mm and ML = 3.0 mm and BA coordinates AP = -1.58 mm and ML = 1.2 mm relative to bregma. Simultaneous optical stimulation and electrical recording in the NBm were carried out using an optrode which consists of an extracellular parylene-C insulated tungsten microelectrode (127-µm diameter, 1 MΩ; A-M Systems) tightly bundled with an optical fiber (200 µm, 0.22 N.A.; Thorlabs), with the tip of the electrode protruding 0.2–0.7 mm beyond the fiber

end to ensure illumination of the recorded neurons as previously described (Shipton et al., 2014). Electrical recording from the amygdala were carried out using a simple extracellular parylene-C insulated tungsten microelectrode (127-µm diameter, 1 MΩ). The optrode was gradually descended into the NBm with a 20° angle. Response to photostimulation was regularly assessed between DV = 3.7 and DV = 4.1 mm to find the best location for an effective stimulation. A common ground electrode for the two electrodes was placed above the right part of the cerebellum and was submersed by saline solution (0.9% NaCl). The recording electrode was descended into the amygdala with a 15° angle to reach a final depth of DV=4.0mm. Light delivery was performed by collimating the optic fibre to a blue laser light (488nm, 15 +/- 3 mW at fiber tip; laser 2000). Light delivery was controlled by a shutter whose aperture was driven by custom-made Igor 6.5 procedures. Electrical signals were amplified and filtered at 0.1–5 kHz (1800 Microelectrode AC Amplifier; A-M Systems), digitized at 20 kHz using an ITC-18 board (Instrutech, Port Washington, NY) and Igor software (Wavemetrics, Lake Oswego, OR). All data were analyzed off-line using Igor Pro 6.37.

Electrophysiology and Analysis:

LFP signal was isolated from high-frequency signals using a low-pass filter cutting frequencies above 120 Hz and the signal was downsampled from 20 kHz to 1 kHz. Each stimulation procedure was repeated at least 20 times with a minimum of 20 s interval between each stimulation. Each recording was submitted to wavelet analysis and the power spectrum over time obtained by the wavelet analysis was z-scored for each frequency over the 20 s of the sweep. (z-score formula = fFreq(t) = (t-meanfreq)/sdFreq. The mean power spectrum for baseline and stimulation conditions was obtained by averaging the power spectrum over 0.5s preceding the stimulation and following the end of stimulation, respectively. Differences of the baseline and stimulation power spectrum were computed using 2-ways ANOVA. For these experiments, 5 ChAT-CRE * Ai32 and 2 transfected ChAT-CRE were used. The variation of the power spectrum between baseline and stimulation conditions was not significatively different between the 2 two pools of animals (2 ways ANOVA, for Amygdala p = 0.09864 and for NBm p = 0.418159).

Immunocytochemistry

To determine the specificity of the opsin expression in the cholinergic neurons, the mice were anesthetized with pentobarbital (500 mg/kg, i.p., Vetoquinol, Buckingham, UK) and transcardially perfused first with 0.1 M PBS followed by 10% neutral-buffered formalin (Sigma, St. Louis, MO, USA). Brains were removed, postfixed overnight at +4°C and cryoprotected at +4°C with 30% w/v sucrose in PBS until the brains sunk. Coronal sections (30 µm) were cut on a freezing sliding microtome (model 860, Americal Optical Company, Buffalo, NY, USA). For both GFP and VAchT immunostaining, the sections were washed at RT in 0.1 M PBS, blocked with 1% BSA (Fisher Scientific, Fair Lawn, NJ, USA) supplemented with 0.3% Triton X-100 (Fisher) in 0.1 M PBS. Sections were then incubated overnight at RT in primary antibodies diluted in blocking buffer, washed in PBS, incubated in secondary antibodies for 2 h at RT, washed in PBS, and mounted on microscope slides and coverslipped. Primary antibodies were chicken anti-GFP (1:1000, ab13970, Abcam, Cambridge, UK) and guinea-pig anti-VAchT (1:500, AB1588, Millipore, Temecula, CA, USA). Secondary antibodies were goat anti-chicken AlexaFluor 488 (1:1000, Abcam) and goat anti-guinea-pig AlexaFluor 594 (1:1000, Abcam). Digital images were captured with a Zeiss Axioskop 2 microscope (Zeiss, Oberkochen, Germany) and QImaging QICAM Fast digital camera (QImaging, Surrey, BC, Canada). Images were merged using ImageJ (National Institutes of Health).

cFos imaging of neuronal activation.

Retrobead injections:

C57Bl/6J mice at the age of 2.5 months were anaesthetised with isoflurane as described previously for viral transduction. A stainless steel bevelled microinjector was lowered to a coordinate aimed at the basolateral amygdala (anteroposterior -1.55 mm in relation to bregma, laterally +/- 2.70 mm in

relation to midline and at –4.90 mm from the skull level) and the central nucleus of amygdala (anteroposterior -1.40 mm in relation to bregma, laterally +/- 2.30 mm in relation to midline and at –4.50 mm from the skull level). Injections were performed by using the same surgical injection system as with the viral transduction. Injection site received 200 nL volume of retrobeads (Lumafluor, Nashville, TN, USA) with a injection rate of 0.1 µL/min followed by a 5-min wait. For postoperative care mice received carprofen (5 mg/kg. s.c., Norbrook, Newry, UK) and a recovery period of 1 week was attained before the behavioural testing.

cFos immunohistochemistry:

To determine the neuronal activation of the retrogradely labelled ChAT-positive cells, triple-labeling cellular imaging was performed for retrobeads, ChAT and cFos. Brain samples were prepared for sections as described above. The sections were washed at RT in 0.1 M PBS, treated for 15 min with 10 mM citrate and for 1 h with hydrogen peroxide, blocked with 3% BSA (Fisher Scientific, Fair Lawn, NJ, USA) supplemented with 0.3% Triton X-100 (Fisher) in 0.1 M PBS. Sections were then incubated overnight at 4°C in cFos primary antibody diluted in blocking buffer, washed in PBS, incubated in secondary antibody for 2 h at RT followed by DAB intensification and washed in PBS. Sections were then incubated in a blocking buffer with 1% BSA supplemented with 0.3% Triton, and incubated overnight at 4°C with a ChAT primary antibody diluted in a blocking buffer, washed in PBS, incubated in secondary antibody for 2 h at RT, and mounted on microscope slides and coverslipped. Primary antibodies were rabbit anti-cFos (1:500, sc-52, Santa Cruz Biotechnology, Santa Cruz, USA) and goat anti-ChAT (1:100, AB144, Millipore, Temecula, CA, USA). Secondary antibodies were biotinylated horse anti-rabbit (1:200, BA-1100, Vector Laboratories, Burlingame, USA) and donkey anti-goat AlexaFluor 488 (1:1000, A-11055, Life Technologies, Eugene, USA). Digital images were captured with a Zeiss Axioimager microscope (Zeiss, Oberkochen, Germany) and Hamamatsu Orca Flash 4.0 digital camera (Hamamatsu, Shizuoka, Japan). Images were merged using ImageJ (National Institutes of Health).

Statistical Analysis:

Averaged data are presented as the mean ± SEM and all data was analyzed using two-tailed statistics. Each animal provided one value with repeated trials (i.e. stimulations) being averaged and the average providing the value for that animal. For cell counts, each n is data from one animal and for cellular ephys each n comes from a single cellular recording. Multiple cells were recorded from an individual animal but at least 3 mice were used for each in vitro dataset.

Figure 1

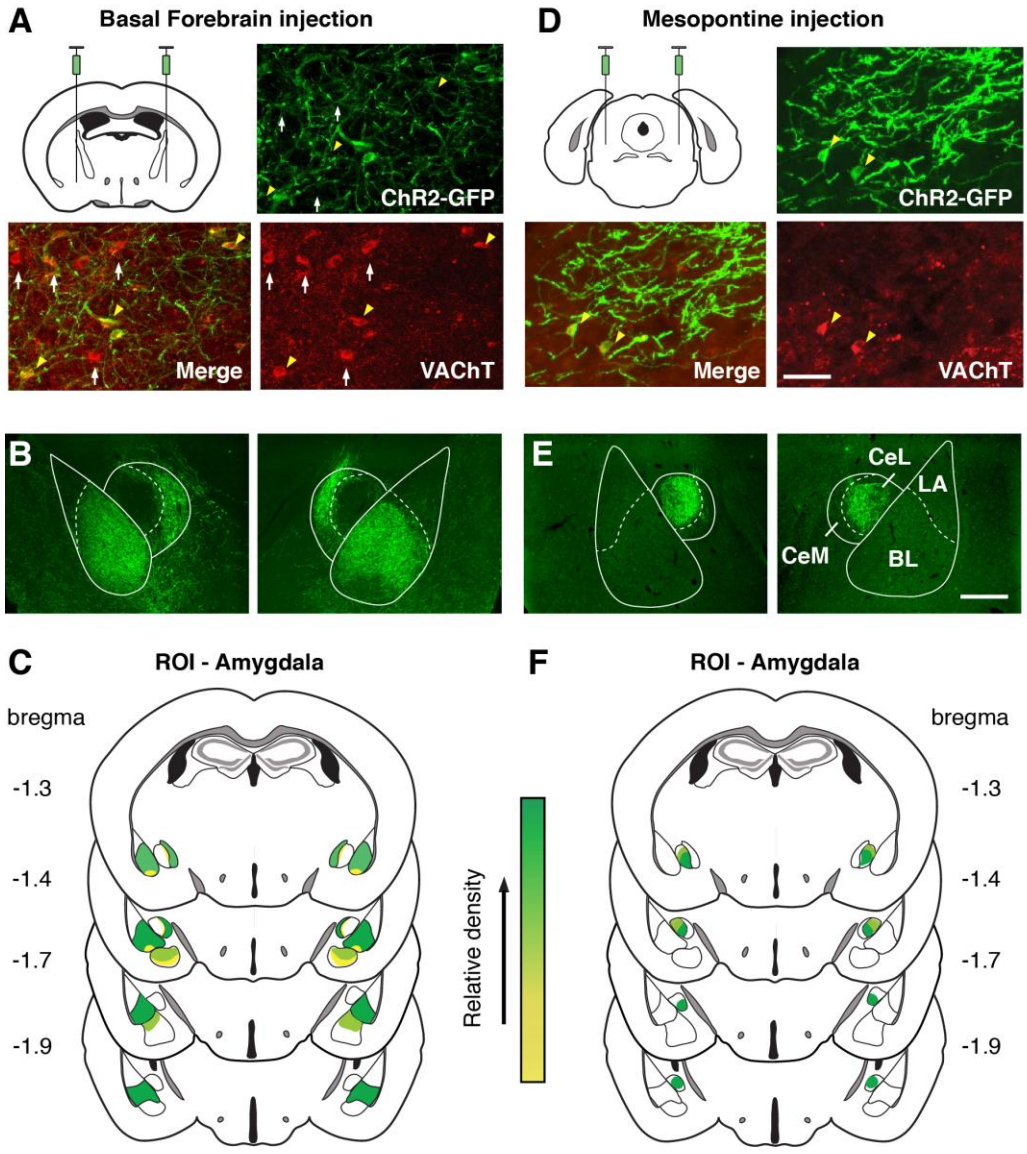

Figure 1: Basal forebrain and Brainstem cholinergic neurons differentially innervate the amygdala. Viral infection of NBm (A) and PPT (D) ChAT-containing neurons in transgenic ChAT-cre mice led to ChR2-GFP expression in local VAChT-expressing neurons (A,D). GFP-labeled fibers of NBm-ChAT neurons mostly innervated the basal and central medial division of the amygdala (B,C) while PPT-ChAT neurons sent projections to the central lateral amygdala nucleus (E,F). C,F. Group summary of BF (C) and PPT (F) distribution in the amygdala plotted as relative density by color. Abbreviations: LA, lateral amygdala; BL, basolateral amygdala; CeL, central lateral amygdala; CeM, central medial amygdala. ROI, region of interest. Scale bars: A, D, 100 μm; B, E, 1 mm.

Figure S1

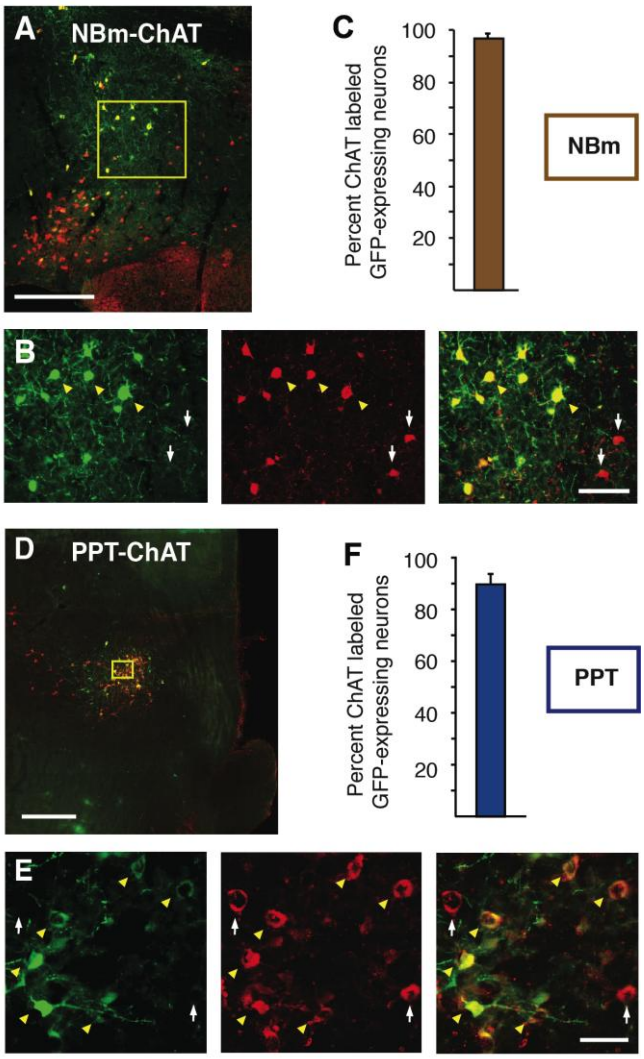

Supp 1: Viral-expression of GFP in ChAT-cre mice is highly specific to ChAT-containing neurons. Low (A) and high (B) magnification images of basal forebrain cholinergic population. Virally-expressed GFP (B; left,right) in NBm ChAT-containing (B; middle, right) neurons. D. PPT viral-injections labeled PPT ChAT-containing neurons with GFP (E; left, right) co-labeled with ChAT (E; middle, right). C,F. Summary data of GFP expression in NBm (C) and PPT (F) ChAT-immunoreactive neurons. White arrows, ChAT-expressing neurons only; yellow arrowheads, GFP and ChAT expressing neurons. Scale bars: A, 200 μm; B, 60 μm; D, 500 μm, E, 30 μm.

Figure 2

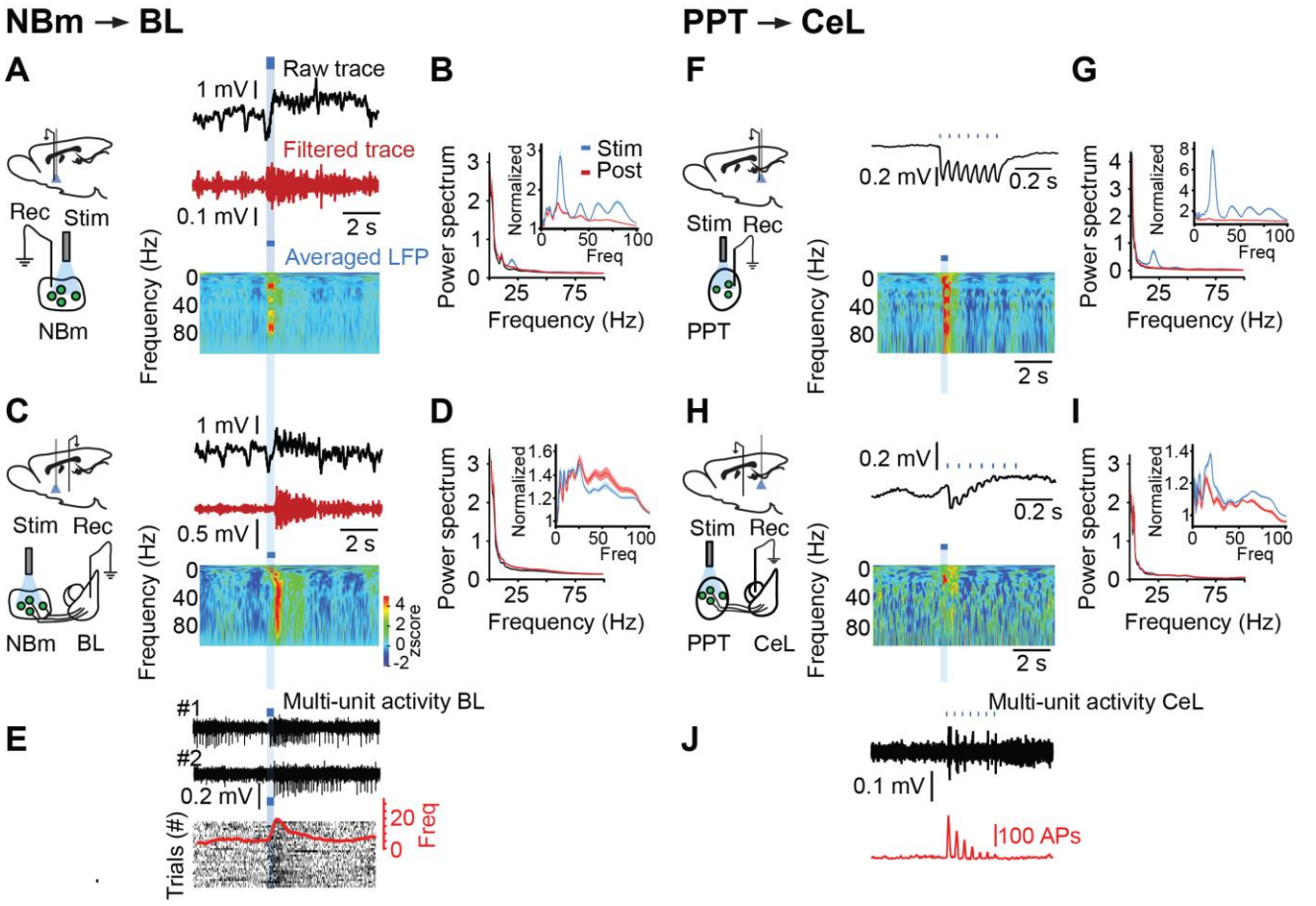

Figure 2: In vivo PPT/NBm photo-activation respectively synchronizes local CeL and BL activity transiently and for seconds after stimulation. NBm-ACh stimulation (n = 10) results in an immediate (A,B) and delayed (C,D) change in NBm and BL local field potentials (LFP), respectively. A,C. Top - right, raw unfiltered LFP; Middle, high-pass filtered LFP; Bottom, color-coded wavelet analysis plotting the frequency power over time (A, NBm; C, BL). Power spectrum of NBm (B) and BL (D) LFP during (blue trace) and immediately after (red trace) stimulation. Normalized NBm (B-inset) and BL (D-inset) power spectrum analysis where the power during (blue trace) and after (red trace) stimulation was divided by the baseline power spectrum. E. (Top) Two separate examples of multi-unit BL activity in response to NBm photo-stimulation. (Bottom) Rasterplot of multi-unit activity recorded during multiple sweeps and their average response (red trace). B-J. Similar analyses for PPT photo-induced responses in the PPT and CeL (n = 6). Photo-driven responses and power spectrum of PPT (F,G) and CeL (H,I) activity. J. PPT photo-evoked multi-unit activity from CeL recordings. Power Spectrum units, mV^2/Hz (B,D; G,I).

Figure S2

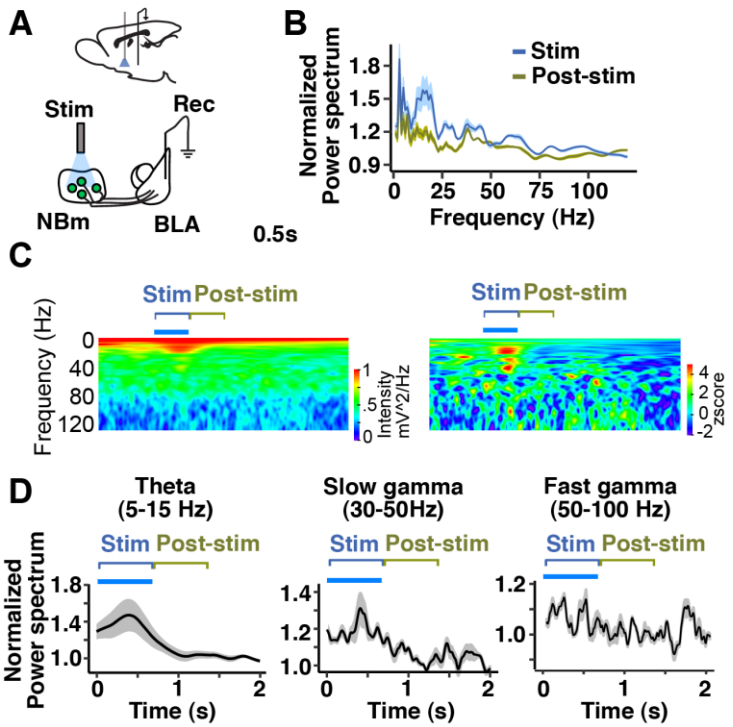

Supp 2: In vivo PPT/NBm photo-activation in awake mice synchronizes BL activity transiently in the theta and gamma frequency band. In freely-behaving mice NBm-ACh stimulation (A) results in an increase in theta and gamma power (B during and after stimulation (C,D). Power Spectrum units, mV^2/Hz (C).

Figure 3

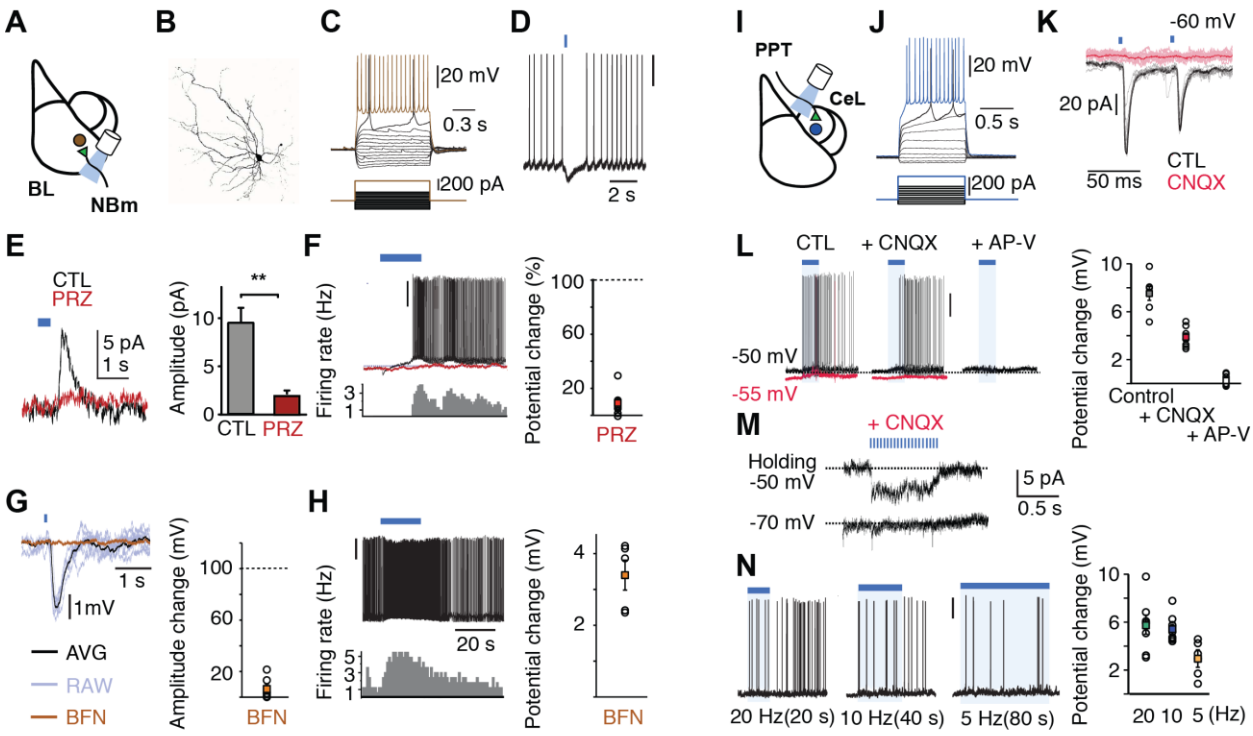

Figure 3: Electrophysiological impact of NBm and PPT cholinergic populations onto BL (A) and CeL (I) activity *in vitro*. A-H. Activation of NBm to BL inputs results in a muscarinic M1 receptor-dependent fast inhibition followed by slow excitation. Morphology (B) Current-voltage relationship (C) and of a BL principal neuron. All recordings showed similar electrophysiological signatures. Optogenetic terminal activation with 1 ms flash of blue light suppressed principal neuron action potentials (D) by increasing a PRZ-sensitive outward K+ conductance (E). In the presence of synaptic blockers, 20 Hz NBm-BL photo-stimulation (20 Hz for 20 sec) led to a PRZ-sensitive slow membrane depolarization in BL principal neurons (F). Occlusion of inwardly-rectifying K^+ channels with the $GABA_b$ agonist baclofen (20 μM) blocked the NBm-BL evoked fast IPSC (G). With baclofen present, 20 Hz NBm-BL photo-stimulation increased BL neuronal firing by depolarizing (3.4 ± 0.4 mV) BL principal neurons (H). I-N, PPT axons directly excite CeL neurons by releasing glutamate that acts postsynaptically on AMPA and NMDA receptors. J, example current-voltage relationship of recorded CeL neuron. K, brief blue light pulses evoked post-synaptic currents that were sensitive to the AMPA receptor antagonist CNQX (20 μM). Stimulation-induced increase in CeL firing frequency (L-left) is composed of an AMPA-mediated (L-middle) and NMDA-mediated (L-right) depolarization, the NMDA response being absent at a more negative membrane potential (M). N, stimulation at 20, 10, and 5 Hz was sufficient to excite CeL neurons.

Figure S3

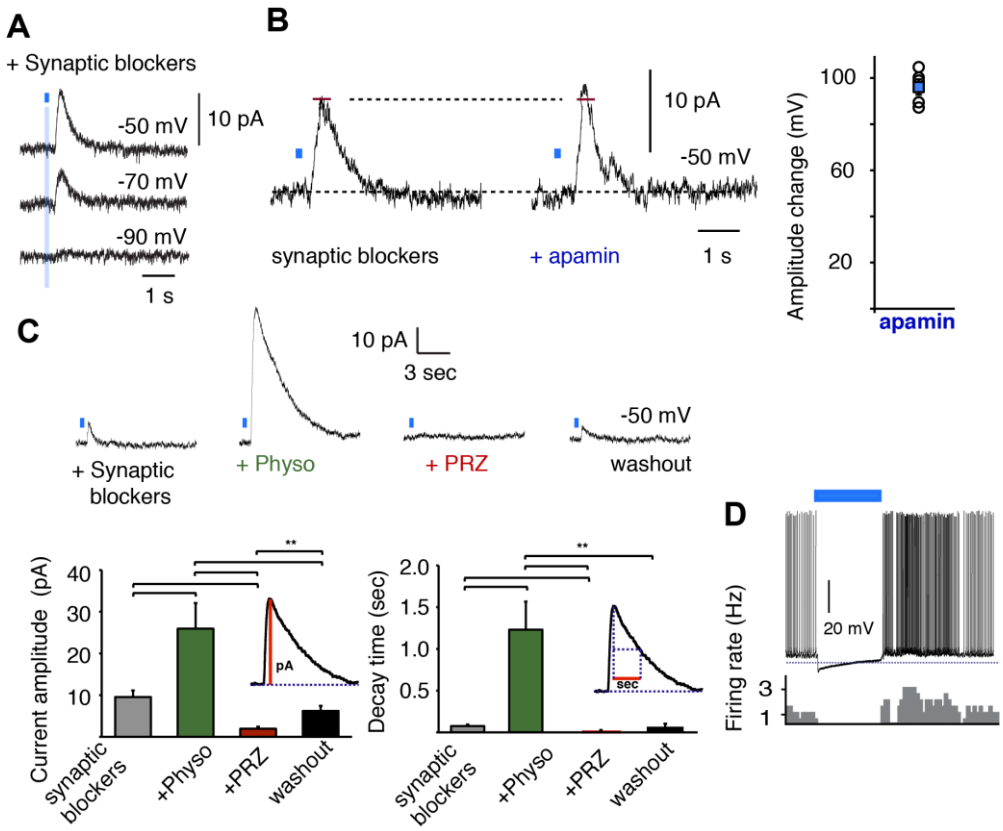

Supp 3: Synaptic properties of NBm inputs onto BL principal neurons. A. inhibitory currents evoked by minimal photo-activation of NBm terminals (0.5 ms flash) (n = 6) in the BL appeared 43.3 ± 2.5 ms after stimulation onset and reversed at approximately -90 mV. These inhibitory currents were unaffected by apamin, the SK Ca^{2+}-activated K^{+} channel blocker (200 nM) (B) but increased in amplitude and duration following application of the cholinesterase inhibitor Physo (10 μM) (C). These responses were subsequently blocked by bath-application of the M1 receptor antagonist PRZ (C). D. In most cases 20 Hz stimulation for 20 seconds resulting in a clear biphasic inhibitory-excitatory response.

Figure S4

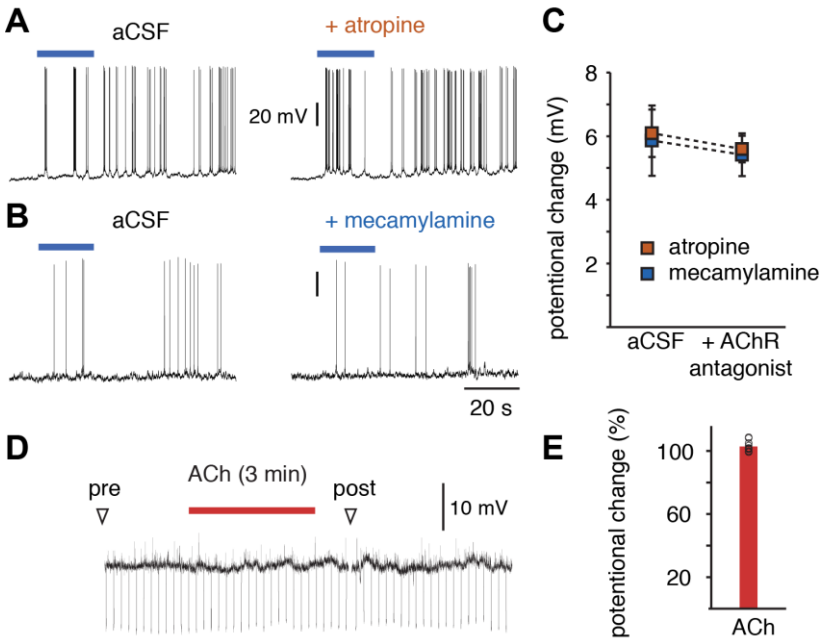

Supp 4: PPT-mediated excitation of CeL neurons is independent of ACh receptor activation. 20 Hz activation of PPT-CeL inputs is unaffected by ACh muscarinic (A,C) and nicotinic (B,C) receptor antagonists (ATR, 2 μM; MEC, 10 μM). D,E. PPT-CeL connected neurons were unresponsive to bath-application of ACh (100 μM).

Figure S5

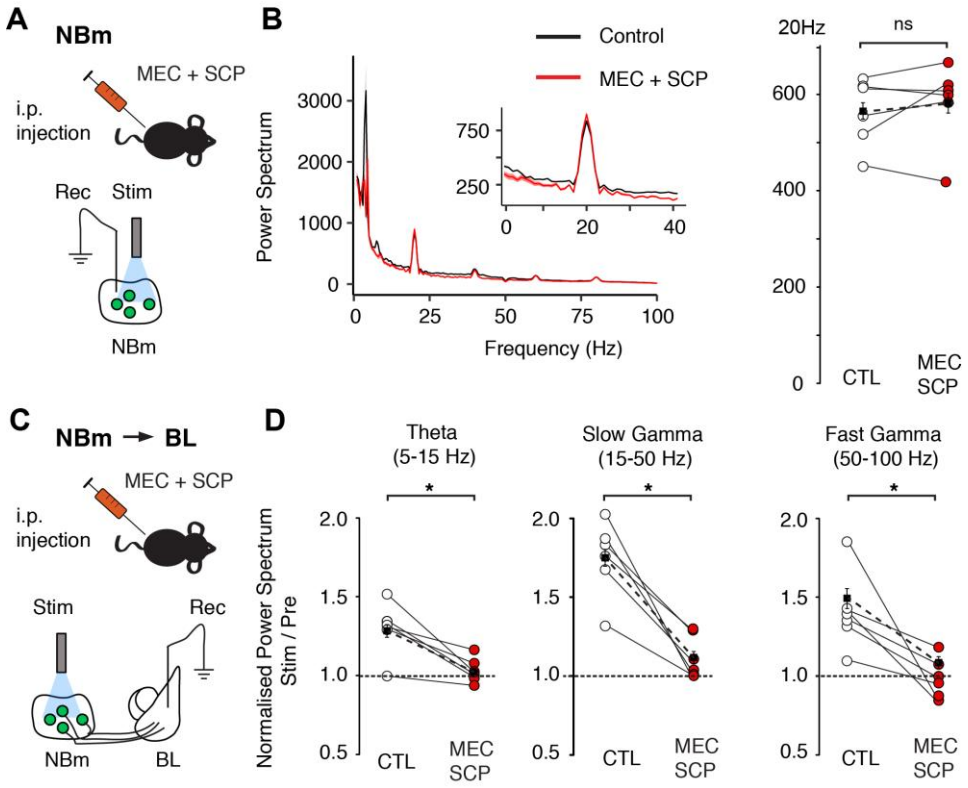

Supp 5: Intraperitonial injection of ACh antagonists diminishes NBm-mediated increase in BL network rhythmicity. A,B. ACh receptor antagonism does not significantly affect the local increase in 20 Hz power in response to 20 Hz photo-stimulation of NBm ChAT-containing neurons. C,D. In contrast, BL responses in different frequency bands (theta, slow and fast gamma) evoked by these same stimulations were significantly reduced by ACh receptor antagonism. Power Spectrum units, (B) $\mu V^2/Hz$.

Figure 4

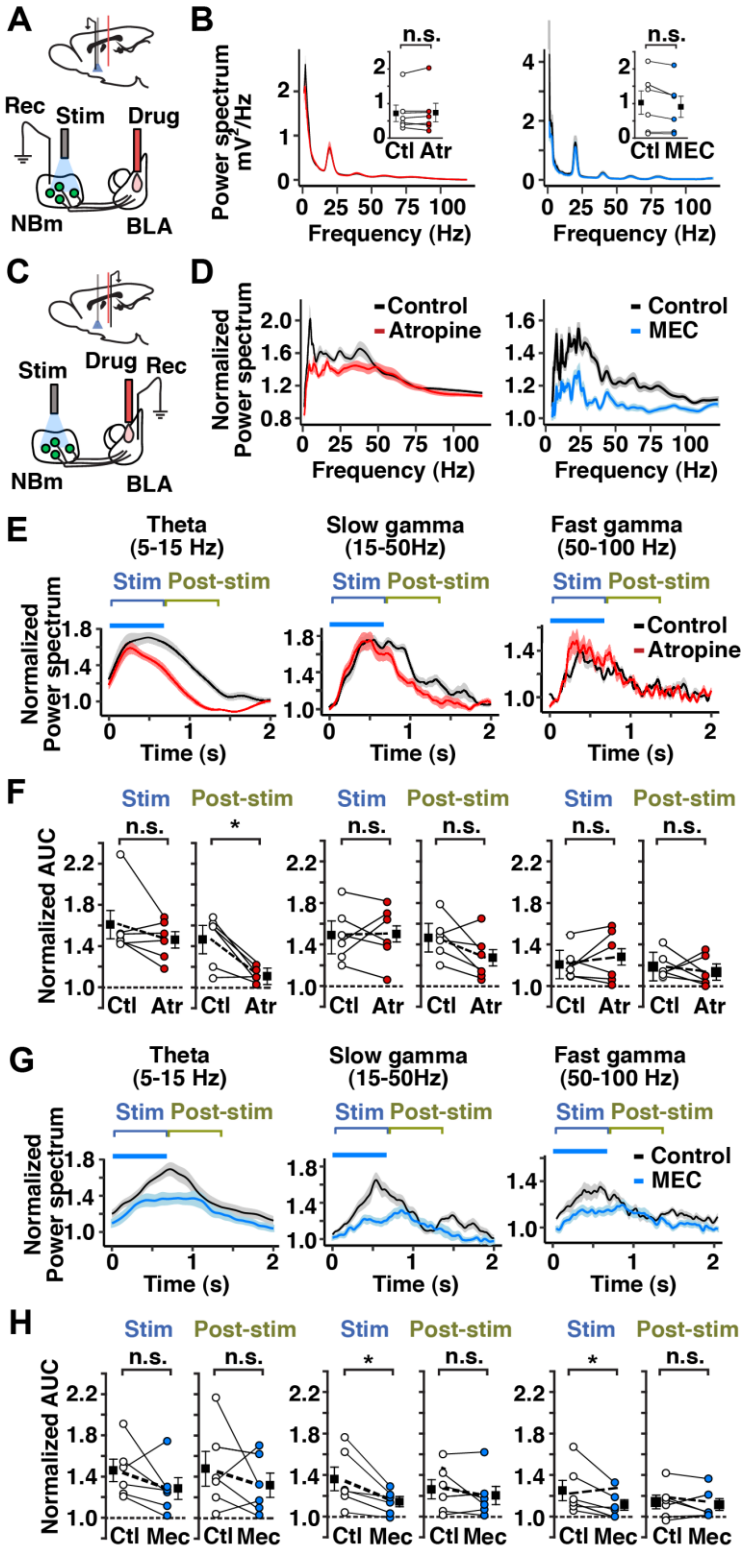

Figure 4: Sustained BL theta rhythmicity in response to NBm-ChAT photo-stimuation is dependent on muscarinic receptor activation while nicotinic receptors contribute to stimulation-induced gamma. A.

BL infusions on the muscarinic and nicotinic receptor antagonists, have no significant impact on the magnitude of NBm field potentials (B). BL infusions of ATR (C) does not significantly alter theta, slow and fast gamma power during stimulation but selectively reduces the magnitude of the ongoing NBm-ChAT evoked BL theta activity (D-left; E,F - left). In contrast, BL infusions of MEC significantly reduces NBm-ChAT evoked slow and fast gamma during stimulation(G, H-middle, right). Power Spectrum units (B), $\mu V^2/Hz$.

Figure S6

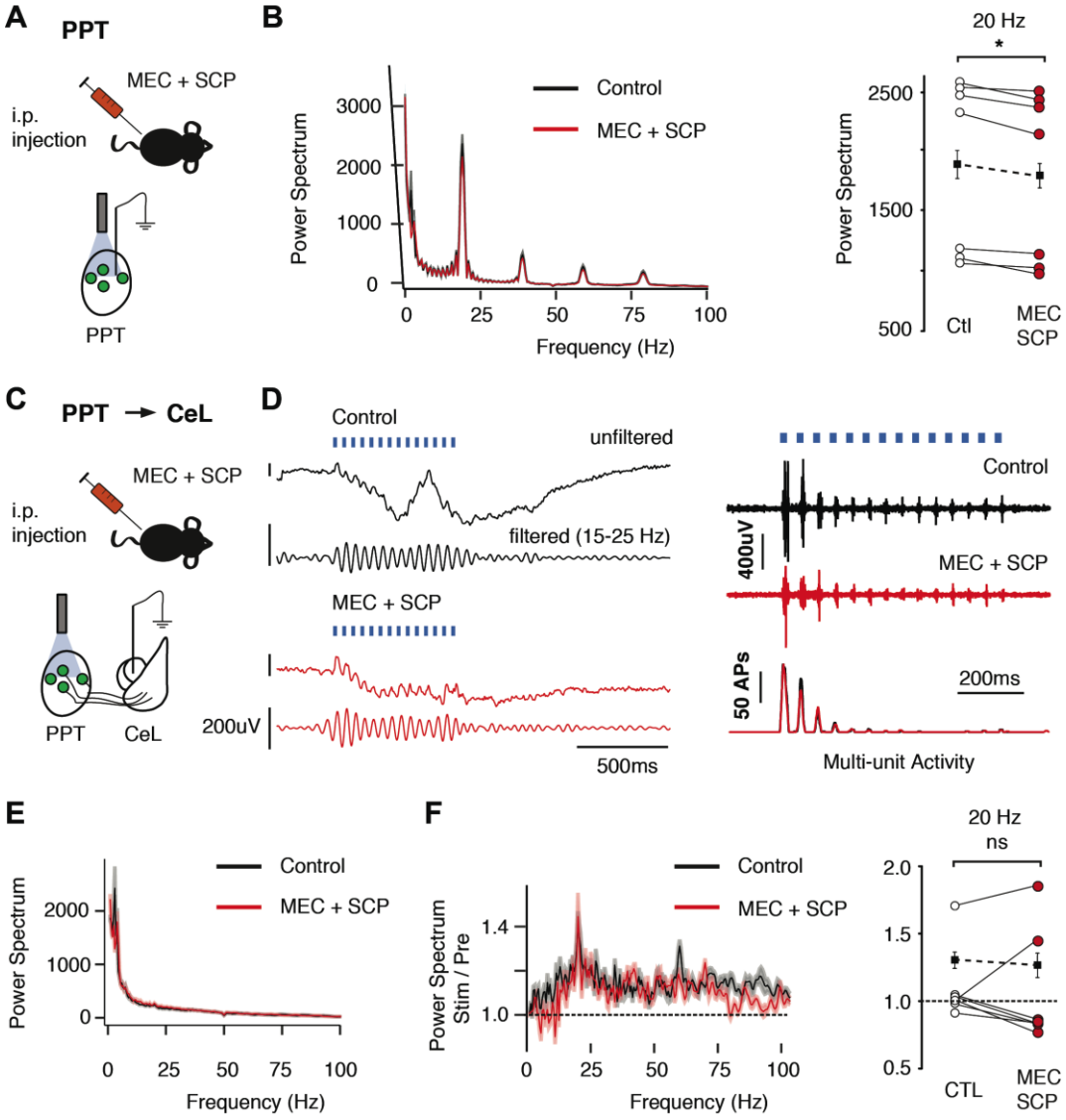

Supp 6: Intraperitonial injection of ACh antagonists diminishes PPT-mediated increase in local activity but has no effect on CeL networks. ACh receptor antagonism (A) significantly reduces the increase in 20 Hz power in response to 20 Hz photostimualtion of PPT ChAT-containing neurons (B-RIGHT). D. PPT-ChAT evoked field (D-left) and multiunit responses (D-right) confined to the CeL. Evoked field potentials were unaffected by ACh receptor antagonism (E,F). Power Spectrum units (B,E), μV^2/Hz.

Figure 5

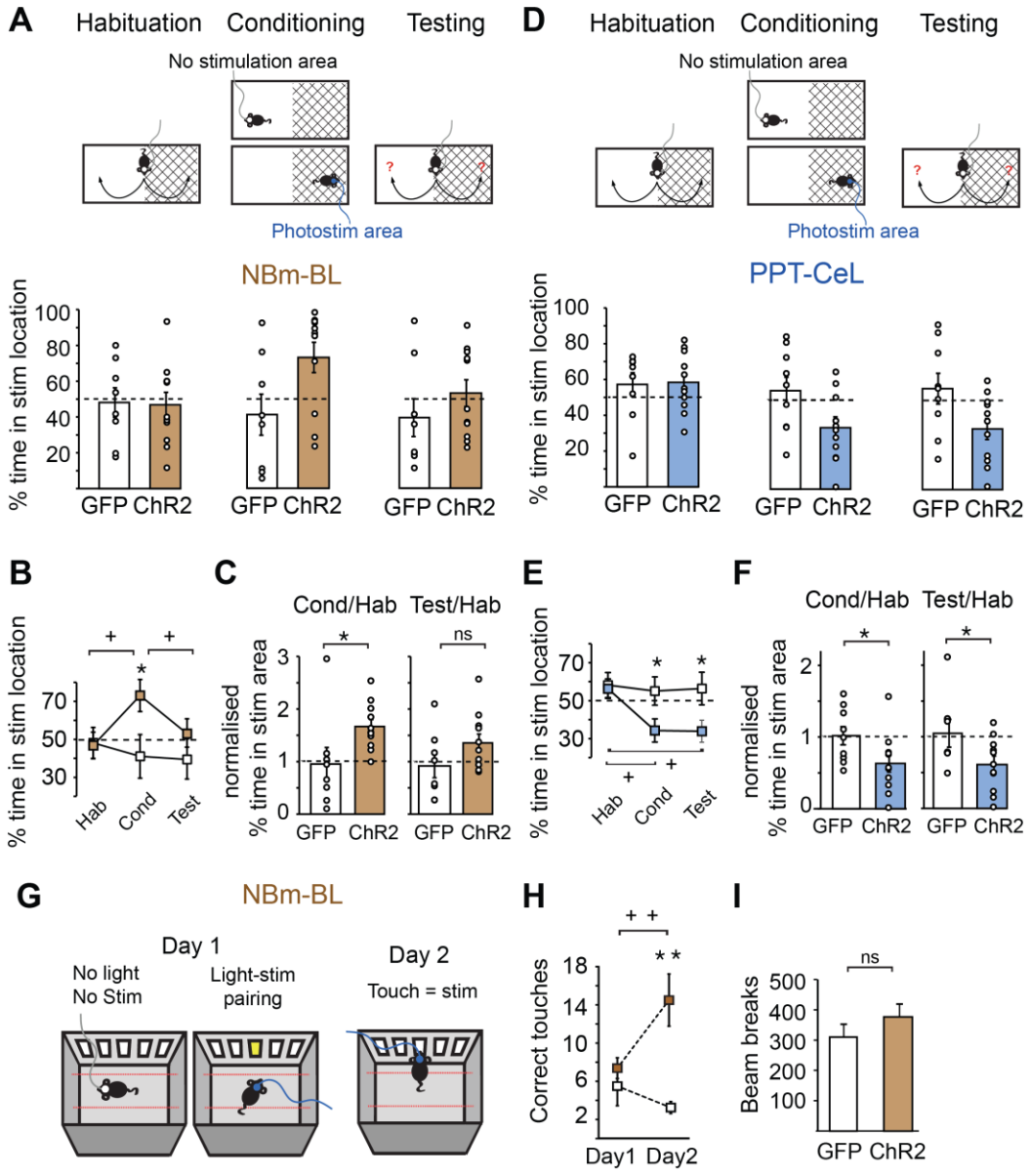

Figure 5: NBm to BL and PPT to CeL inputs, respectively, drive approach and avoidance behavior. A,D. (top) Schematic of the place preference paradigm where animals underwent a habituation, conditioning, and testing phase and raw data (circles) including averages (bar), of the time spent in the stimulation area for all phases in NBm-BL (A, bottom) and PPT-CeL (D, bottom) mice. In the place preference paradigm, ChR2-exprerssing mice receiving NBm-BL stimulation spent an equal amount of time in each region during the habituation phase but spent less time than control GFP-expressing mice in light-paired region during stimulation (B). For NBm-BL ChR2 mice, the ratio of stim time spent in conditioning phase over time spent in the habituation phase was significantly greater than GFP

mice (C). Mice receiving PPT-CeL stimulation similarly showed no region-selective difference during the habituation phase but instead spent less time than control mice in only the light-paired region during the conditioning and testing phases (E). For PPT-CeL ChR2 mice, the ratio of stim time spent in both conditioning and testing phases over time spent in the habituation phase was significantly less than GFP mice (F). G. Schematic of the self-stimulation paradigm. On Day 1 mice received center screen light photo-stimulation pairings. On Day 2 mice received photo-stimulation only when the center touchscreen was touched. On Day 1 of a self-stimulation paradigm, ChR2 (n = 8) and GFP (n = 6) mice touched the paired touch screen an equal number of times while on Day 2 ChR2 mice correctly touched more than GFP-control mice. C3 (H). Locomotor activity as measured by beam breaks was no different in control and ChR2 groups (I).

Figure S7

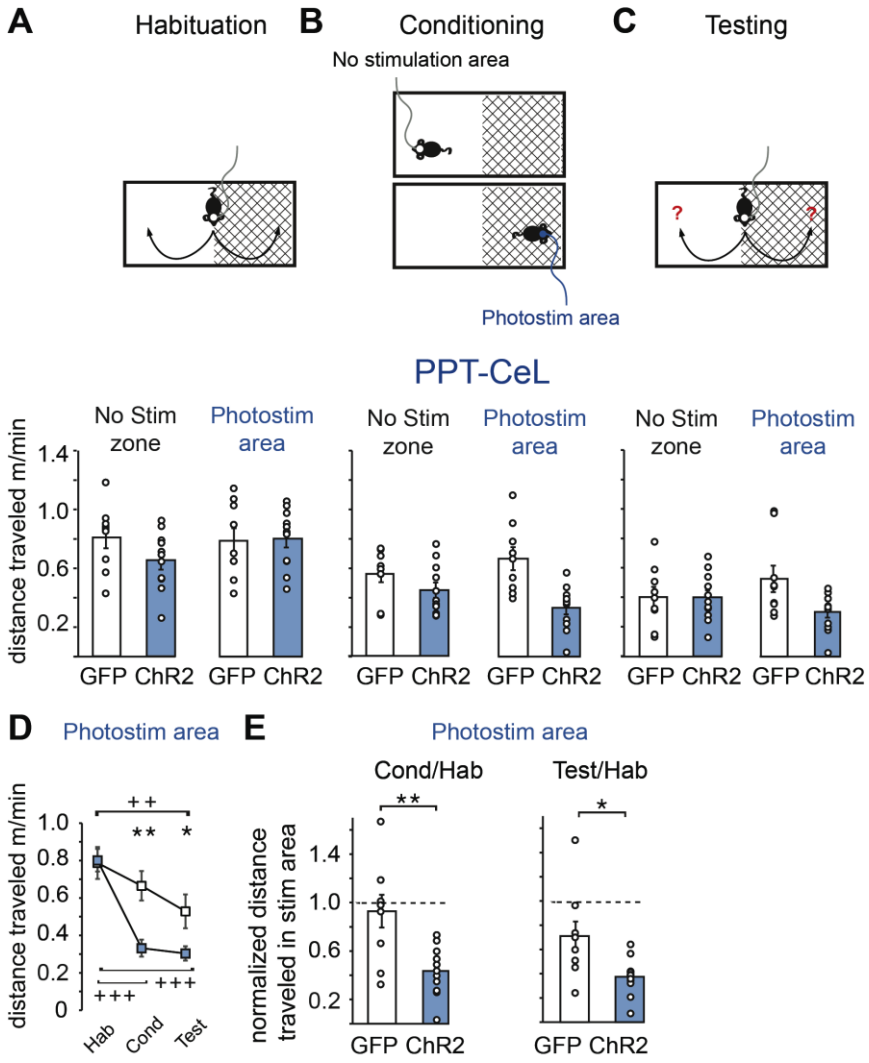

Supp 7: PPT-CeL activated mice were less active during place preference conditioning. A-C. Schematic of the place preference paradigm where animals underwent a habituation, conditioning, and testing phase (top) and raw data (circles) including averages (bar), of exploration speed (m/sec) for all phases in PPT-CeL mice (bottom). When in the stimulated area, PPT-CeL activated mice showed a significant reduction in speed during both conditioning and testing phases compared to the habituation phase and to GFP control mice (D). In the stimulation area, the rate of movement of ChR2 animals in both conditioning and testing phases normalized by their speed during the habituation phase was significantly less than GFP mice (E).

Figure 6

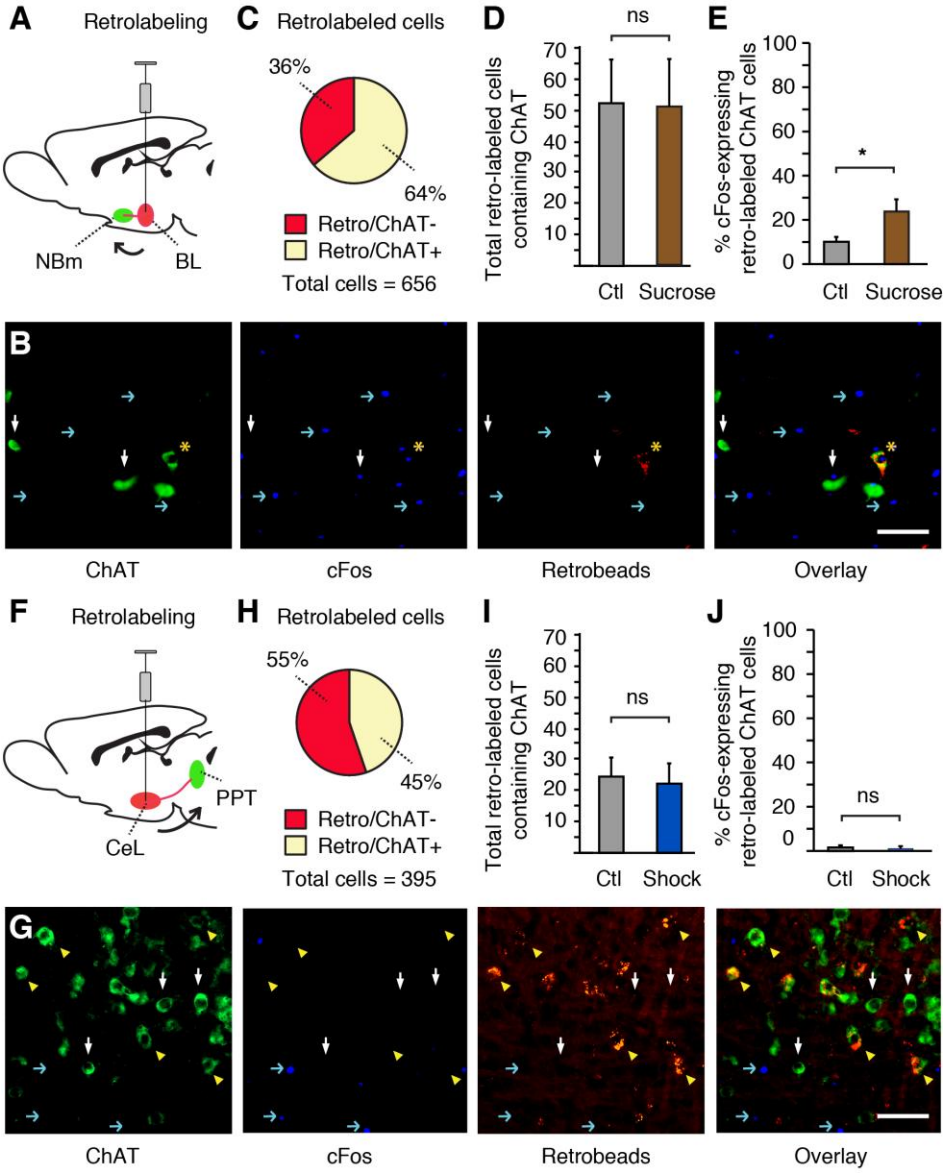

Figure 6: Appetitive stimulus activates BL-projecting NBm ChAT neurons. A. BL injections of retrobeads retro-labeled both ChAT+ and ChAT- NBm neurons (B,C). In control and sucrose-exposed mice, there was an equal amount of NBm-projecting ChAT+ neurons (B,D). Sucrose exposed mice however had a greater amount of retro-labeled NBm ChAT neurons express cFos than control mice (E). F. CeL injections of retrobeads retro-labeled both ChAT+ and ChAT- PPT neurons (G,H). Control and foot-shock exposed mice had similar amounts of CeL-projecting ChAT neurons in the PPT (G,I). Mice receiving footshocks showed no difference in the amount of retrolabeled PPT ChAT neurons that express cFos compared to control mice (J). White arrows, ChAT-expressing neurons only; blue arrow, cFos; yellow arrowheads, retrogradely-labeled ChAT expressing neurons; yellow star, retrogradely-labeled ChAT neurons expressing cFos. Scale bars: B, G, 50 μm.

Figure S8

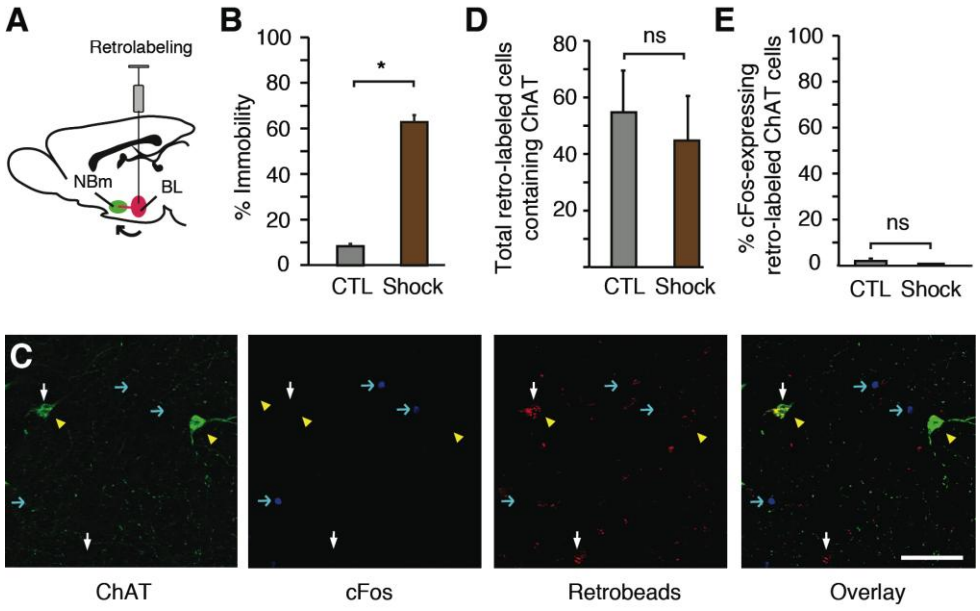

Supp 8: Aversive stimulus does not activate BL-projecting NBm ChAT neurons. BL injected mice with reotrobeads (A) expressed fear-related behavior (immobility) when presented with unpredicted footshocks (B). BL injections of retrobreads labeled NBm-ChAT neurons equally in control and footshock-exposed mice (C,D). No difference in cFos expression was seen between the groups (E). Scale bars: C, 50 μm.